WILLIAM & MARY
CHARTERED 1693

W&M ScholarWorks

Undergraduate Honors Theses

Theses, Dissertations, & Master Projects

4-2019

Impacts of Harmful Algal Blooms on Dissolved Organic Carbon in the Lower York River Estuary

Joshua Sacks

Mark J. Brush
Virginia Institute of Marine Science

Iris C. Anderson
Virginia Institute of Marine Science

Follow this and additional works at: https://scholarworks.wm.edu/honorstheses

Part of the Analytical Chemistry Commons, Biogeochemistry Commons, Environmental Chemistry Commons, Marine Biology Commons, Oceanography Commons, and the Terrestrial and Aquatic Ecology Commons

Recommended Citation

Impacts of Harmful Algal Blooms on Dissolved Organic Carbon in the Lower York River
Estuary
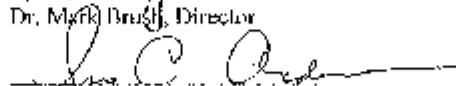
A thesis submitted in partial fulfillment of the requirement
for the degree of Bachelor of Science in Interdisciplinary Studies from
The College of William and Mary

by

Joshua Sacks

Accepted for ___Highest honors___
(Honors, High Honors, Highest Honors)

Dr. Mark Brush, Director

Dr. Iris Anderson, Director

Dr. Rachel O'Brien

Williamsburg, VA
April 29, 2019

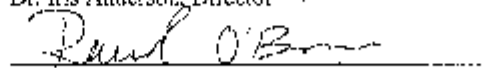Title: Impact of Intense Algal Blooms on Dissolved Organic Carbon in the Lower York River Estuary

Authors: Joshua Sacks, Dr. Mark Brush, Dr. Iris Anderson

Table of Contents:

Abstract:

Estuaries are important sites of carbon cycling; however, the impact of increasingly prevalent harmful algal blooms (HABs) on cycling in these systems remains unclear. To examine the impact of two bloom species, *Alexandrium monilatum* and *Margalefidinium polykrikoides* on the quantity and composition of the dissolved organic carbon (DOC) and chromophoric dissolved organic matter (CDOM) pools and rates of benthic and pelagic microbial respiration in the lower York River Estuary, VA, a series field samplings and laboratory incubations were performed. The two HAB species greatly increased the size of the DOC and CDOM pools and altered the character of the CDOM pool, causing it to shift towards higher molecular weights and lower levels of aromaticity. DOC released by *A. monilatum* and *M. polykrikoides* both stimulated increased respiration by pelagic microbes, but displayed different levels of microbial lability in the DOC produced suggesting species level differences in how HABs affect DOC cycling. HAB produced organic matter did not stimulate increased levels of benthic microbial respiration as measured in sediment core incubations, suggesting that benthic microbial communities are not carbon limited. These findings show that HABs alter the quality and quantity of the DOC pool which in turn affects pelagic microbial respiration. This study also highlighted the need for species level analysis of HABs to be factored in to future estuarine carbon budgets in HAB affected systems.

Acknowledgements:

I would like to sincerely thank my advisors, Dr. Mark Brush and Dr. Iris Anderson for their support, enthusiasm, and guidance throughout this project. I would also like to thank Dr. Kim Reece, Hunter Walker, Bill Jones, Michelle Woods, Stephanie Peart, and Derek Detweiler for their assistance in lab and field work. I would also like to thank Dr. Rachel O'Brien for being a part of my thesis committee. I would like to thank the National Science Foundation for the funding that made this project possible. Finally, I would like to thank my parents for their support throughout this project, for always encouraging me to challenge myself, and for inspiring a love of marine science.

Introduction:

Estuaries are key sites of organic carbon production, remineralization, and transformation and serve as the primary interface between terrestrial and marine carbon cycles (Canuel et al. 2012). Estuaries can serve as important sources of organic carbon to the coastal ocean by exporting both allochthonous, terrestrially-produced carbon from runoff as well as autochthonous, marine-produced organic carbon from within the estuary itself. However, in some estuaries, remineralization by pelagic and benthic estuarine bacteria result in a net production of inorganic carbon by the system resulting in the export of dissolved inorganic carbon to the coastal ocean and degassing to the atmosphere (Bauer et al 2013). The large number of complex and interrelated input, export, and transformation terms in the estuarine carbon cycle along with the substantial diversity in estuary types make estuaries a major source of uncertainty for global carbon budgets (Canuel et al. 2012).

Carbon in marine systems is classified as either inorganic (dissolved CO_2, bicarbonate, and carbonate species) or organic. The organic carbon pool can be separated into two fractions: particulate organic carbon (POC) and dissolved organic carbon (DOC) that is operationally defined as passing through a filter of a certain size. DOC is a highly complex mixture with numerous factors affecting its concentration and composition. Understanding the heterogeneous nature of the DOC pool is essential to understanding its lability, or how easily it is broken down, by biological and physical processes (Hansell and Carlson 2014). A subsection of the DOC pool can be further categorized as chromophoric dissolved organic matter (CDOM), which is comprised of high molecular weight and more aromatic dissolved organic molecules that are able to interact with light. CDOM is typically considered a terrestrial signature in estuaries and it has

been used as a tracer of allochtonous DOC (Helms et al. 2008, Helms et al. 2014, Leech et al. 2016).

The production, processing, and remineralization of DOC is an important component in determining if an estuary is a net source of CO_2 (net heterotrophic) or a net sink of CO_2 (net autotrophic). Assessments of the net ecosystem metabolism of estuaries on the east coast of the United States in general have been varied and without consensus (Canuel et al 2012, Van Dam et al. 2018). Improving the understanding of DOC cycling in these estuaries may help constrain some of these estimates and reveal important factors to consider in current and future monitoring efforts. Furthermore, the rapid respiration of DOC, particularly that produced by algal blooms, can contribute to hypoxia in certain regions, making understanding of its cycling even more important for ensuring ecological health (Heisler et al 2008). CDOM is of additional interest since it can interact with potentially biologically important or toxic metals as well as organic pollutants (Hansell and Carlson 2014). CDOM, through its light absorbing properties, can cause shading for primary producers in the water column and the benthic environment. However, the interactions between light and CDOM can also lead to its breakdown through photodegradation (Vähätalo and Wetzel 2004).

One of the largest potential perturbations to the ecology and biogeochemistry of estuaries are intense algal blooms. During these blooms, phytoplankton reproduce rapidly and accumulate large amounts of biomass which can negatively impact the ecosystem, resulting in their designation as harmful algal blooms (HABs) (Heisler et al 2008). Some species, such as *A. monilatum*, also release toxins that can be harmful to marine organisms (Harding et al. 2009). These blooms result in large increases in carbon fixation through photosynthesis that can likely alter the size and character of the DOC pools in the estuary as pelagic primary production

temporarily becomes the largest input term. Four important loss or transformation terms for DOC in estuaries are export to the coastal ocean, respiration by pelagic microbes, respiration by benthic microbes, and photodegradation (Bauer et al. 2013). DOC exported to the coastal ocean is typically the most refractory and, therefore, resistant to decomposition by microbes; large, complex, photolabile CDOM is most susceptible to photodegradation (Bauer et al. 2013). The impact of HABs on carbon cycling in the estuary will largely be determined by their impact on the DOC pool and how the character of the DOC produced affects its partitioning between the four main export terms.

DOC and CDOM produced by phytoplankton in estuaries is considered to have lower molecular weights, lower levels of aromaticity, lower levels of photodegradability, and higher levels of bioavailability to microbial decomposition when compared with DOC and CDOM that is terrestrial in origin (Helms et al. 2008). However, these studies typically examined seasonal or geographic changes in DOC and some studies focused on blooms have documented the production of CDOM by HAB species (Yamashita et al 2010, Leech et al 2016, Suksomjit et al. 2009). Additionally, studies have doccumented differential impacts on DOC and CDOM pools by various species, suggesting that species specific studies may be required to accurately characterize the impact of blooms on carbon cycling (Castillo et al. 2010, Suksomjit et al. 2009).

The Lower York River Estuary, VA, a tributary of the Chesapeake Bay, experiences a sequence of nearly annual harmful algal blooms that last for roughly four weeks in late summer. The bloom species are *M. polykrikoides* and *A. monilatum*. Both species are dinoflagellates and typically reach cell counts between 10,000 and 100,000 cells/mL in August (Marshall and Egerton 2009). *M. polykrikoides* blooms first and is followed by *A. monilatum* several weeks

later. Preliminary results indicate that these HABs do increase the DOC pool but the nature of this impact remains unclear (Anderson et al. unpublished data).

Harmful algal blooms have been shown to drastically alter the DOC and CDOM pools of marine environments and are becoming increasingly important events in estuaries throughout the world. However, the species-specific impacts of blooms on DOC and microbial metabolisms in estuaries has not yet been characterized. This study sought to identify the impacts of *M. polykrikoides* and *A. monilatum* on the DOC pool in the lower York River estuary through a series of field and lab experiments to address the following hypotheses: H1: Algal blooms will greatly increase the quantity and alter the quality of the DOC pool; H2: The large quantities of DOC produced by algal blooms will be highly labile and stimulate increased pelagic microbial respiration; H3: The large quantities of DOC produced by the blooms will stimulate respiration by benthic microbes.

Methods:

Study Site:

The York River Estuary is a tributary to the Chesapeake Bay in Virginia formed by the confluence of the Pamunkey and Mattaponi Rivers (Shen and Haas 2004; Lake and Brush 2015). The downstream area where the river connects to and mixes with the Chesapeake Bay forms the Lower York River Estuary (LYRE) (Figure 1). The LYRE is a shallow, microtidal system with shoals less than 2 m deep making up approximately 40 % of the estuarine area (Rizzo and Wetzel 1985). The LYRE is subject to anthropogenic nutrient pollution that contributes to the primary production and carbon cycling in the estuary.

The LYRE receives organic matter and nutrient inputs from a combination of near-field sources such as runoff from adjacent forests, wetlands, and agricultural land, far-field sources such as the Pamunkey and Mattaponi Rivers and the Chesapeake Bay, and autochthonous sources within the estuary such as phytoplankton and microphytobenthos (Lake and Brush 2015). During the summer, autochthonous phytoplankton inputs have been identified as the main source of organic carbon to the LYRE (Lake et al. 2013).

Experimental Design

This study was composed of three experiments. First, *in situ* samples taken during blooms of *A. monilatum* and *M. polykrikodies* during August 2017 were used to identify changes to the DOC pool during the blooms. In June-November 2018, laboratory cultures of *A. monilatum* and *M. polkrikodies* were used to confirm the impacts of the bloom species on the DOC pool and to examine the microbial breakdown of the DOC. A third set of experiments was completed in October 2018 examining the impacts of the blooms on benthic respiration using sediment core incubations.

In-situ Analysis:

In August 2017, dissolved organic carbon (DIC), DOC, and CDOM samples were collected at sites in and out of the blooms in the LYRE. The LYRE was sampled once a week for four weeks to document the entire life cycle of the blooms. These samples were collected in triplicate from the surface at 10 stations starting at the mouth of the LYRE and moving upstream (Figure 2). The water samples were collected from a submersible outflow pump 0.5 m below the surface. Samples were filtered (0.45 µm polysulfone) on site and stored on ice before being

either frozen or refrigerated upon returning to VIMS. Cell counts were provided by Dr. Kimberly

Reece.

Microbial Decomposition Experiments:

To confirm the quantitative and qualitative impacts of *A. monilatum* and *M. polykrikodies* on the DOC pool and determine the bioavailability of the DOC produced by the bloom organisms, a series of incubations using laboratory cultures of the two species were performed. Samples (800 ml) taken from the bloom cultures were filtered through 2.7 µm GF/D glass fiber filters to remove all phytoplankton and combined with 1000 ml of sterile culture media. The diluted sample was then filtered through a 0.2 µm polyethersulfone membrane filter to remove particulate matter and bacteria present, and 300 ml of the filtrate was placed into sterile 1 L Tedlar gas sampling bags fitted with polypropylene spigots using sterile 60 mL plastic syringes. Culture media, filtered through 0.2 µm polyethersulfone membrane filters and placed in the gas sampling bags as above, served as controls. A bacterial inoculum (30 ml), collected by filtering York River water through a combusted glass fiber filter (0.7µm), was stored overnight at 4 ˚C and added to each bag. The bags were incubated in the dark in an environmental chamber held at a constant 27 ˚C for two weeks with samples for DOC, DIC, and CDOM analyses collected at the beginning and end of the experiment. Samples were collected by withdrawing water from the bags through the spigots using sterile syringes.

Sediment Core Incubations:

Two sets of six sediment cores each were collected from the LYRE (Figure 1) in clear acrylic tubes (13.3 cm ID x 40 cm tall) to a depth of 20 cm. Upon collection, the cores were capped and transported back to an environmental chamber and allowed to equilibrate uncapped

for 18 hours in water collected from the same location at 23 °C. After 18 hours, cores were removed from the water bath, and all water was removed from the headspace above the sediment using a plastic syringe.

Cells of *A. monilatum* for trial 1 and *M. polykrikodies* for trial 2 were filtered out of their respective cultures using a 2.7 µm GF/D glass fiber filter, sonicated to kill any living cells, and resuspended in 2.7 µm filtered LYRE water. The resuspended cells were then added to three cores (three cores for each species) using a plastic syringe; filtered York River water without cells was added to the other three cores as the control. The cores were then capped, placed in a ventilated laboratory hood for *A. monilatum* and in a dark environmental chamber for *M. polykrikodies*, and allowed to equilibrate for an additional hour to allow for some suspended particulate matter to settle. Magnetic stirrers were used to gently mix water in the headspace of the cores to prevent the development of chemical gradients. The cores were incubated in the dark at 23 °C for six hours with DOC and DIC samples collected at the beginning and end of the incubation. DOC and DIC samples were collected by removing the acrylic lids and gently sampling the water above the cores without disturbing the sediment layer using sterile syringes.

Sample Processing:

DOC:

15 ml of water were filtered through a 0.45 µm polysulfone filter into 20 ml pre-combusted glass scintillation vials and frozen until analysis by high temperature catalytic oxidation on a Shimadzu TOC-V CSN total organic carbon analyzer. A calibration curve was created for this instrument using potassium hydrogen phthalate,

DIC:

Samples were stored in 12.8 mL gas-tight, glass hungate vials spiked with 8 µL of saturated

mercuric chloride ($HgCl_2$) solution. These samples were then stored inverted and submerged in

water at 4 ˚C until analysis on an Apollo SciTech dissolved inorganic carbon analyzer model As-

C3. Sample (50 µl) was introduced via a sipper into a solution of 0.05 M H_2SO_4, and sparged

with N_2 gas, which swept the CO_2 produced to a Li-COR 700 infrared gas analyzer for

determination of concentration. CO_2 in seawater reference material prepared by the Scripps

Institution of Oceanography was used to relate the signal from the sample to the amount of DIC

present. The calibration curve was created using five different concentrations of Na_2CO_3 from

500 µM to 3000 µM with check standards used every 10 samples to identify any drift. Analytical

replicates were analyzed until good agreement (a difference of less than 1%) was observed

between runs, usually between three and five (Neubauer and Anderson 2003).

CDOM:

CDOM samples (10 ml), collected from the Tedlar bags, were filtered through 0.45 µm

polysulfone filters into whirl-pak bags and frozen until analysis on a Beckman Coulter DU 800

spectrophotometer. Deionized water was used as blanks with two blanks run for every 10

readings. Full spectrum UV-Vis absorption scans (200-750 nm) were performed on each sample

in duplicate. For every 10 readings, the two blanks were averaged and subtracted from the

absorbance values at each wavelength. The absorbance at 750 nm was then subtracted from that

of all other wavelengths. These corrections removed background noise and accounted for any

baseline drift in the instrument (Leech et al. 2016). The Napierian absorption coefficients for

each wavelength of each sample were then computed using the equation:

$$a_\lambda = 2.303 \times A_\lambda / l$$

where a_λ is the Napierian absorption coefficient (m^{-1}), A_λ is the corrected absorbance at wavelength λ, and l is the pathlength, in this case 0.01 m. The absorption coefficient at 350 nm was used as the measurement of CDOM in this study (Leech et al 2015).

Optical Proxies

A variety of optical proxies were used to qualitatively assess the DOC pool for characteristics such as molecular weight, aromaticity, and photodegradability. The first proxy, slope ratio (S$_R$), was determined using the equation:

$$S_R = \frac{S_{\ln(275)-\ln(295)}}{S_{\ln(350)-\ln(400)}}$$

where $S_{\ln(275)-\ln(295)}$ is the linear slope of the natural log of Napierian absorption coefficients at 275 nm and 295 nm, and $S_{\ln(350)-\ln(400)}$ is the linear slope of the natural log of Napierian absorption coefficients at 350 nm and 400 nm. This ratio has been closely correlated with CDOM molecular weight and photodegradability with higher S$_R$ values being indicative of lower molecular weight, less photodegradable material which is typically thought of as being representative of CDOM pools that are more marine in origin (Helms et al. 2008). Lower S$_R$ values typically indicate a CDOM pool that is on average higher molecular weight, more photodegradable, and more terrestrial in origin.

The ratio of the Napierian absorption coefficients at 254 nm and 365 nm was also computed. Higher molecular weight organic carbon species absorb light at longer wavelengths to a greater extent than lower molecular weight species. The ratio of the absorption at these two wavelengths is therefore correlated with molecular weight, with higher $a_{254}:a_{365}$ values being

indicative of a lower average molecular weight of the CDOM pool (De Haan and De Boer 1987; Leech et al. 2016).

The third optical proxy used was specific UV absorbance at 254 nm ($SUVA_{254}$). This is calculated by dividing the Napierian absorption coefficient at 254 nm by the concentration of DOC in μM. This serves as a proxy for CDOM aromaticity with higher $SUVA_{254}$ values being indicative of a higher average degree of aromaticity of the CDOM pool (Weishaar et al. 2003). Aromaticity has been shown to serve as a predictor of photolability as conjugated rings and other aromatic structures tend to be highly reactive with light (Helms et al. 2014).

Results:

In situ measurements:

M. polykrikoides Bloom: August, 9th, 2017

A bloom of *M. polykrikoides* was documented on a cruise on August, 9th, 2017. The cruise sampled stations with bloom densities that ranged from 0 to 32,954 genomes/mL with three sampling stations having greater than 15,000 genomes/mL. The bloom was documented primarily upstream from the mouth of the LYRE. DOC values (Figure 3) ranged from 275 to 849 μM and were highest at stations with greater *M. polykrikoides* density. CDOM values (Figure 4) were measured as absorbance at 350 nm and ranged from 2.21 to 6.61 m^{-1}. CDOM and DOC followed a similar pattern to the density of *M. polykrikoides*: highest at stations 5, 6, 8, and 10 and very low at stations 1-4. A linear regression model, which was used to compare the density of *M. polykrikoides* to DOC (Figure 13) and CDOM (Figure 14), showed a strong, positive, linear trend with DOC; 84.5% of the variation in DOC concentration was explained by the

density of the bloom. A similar, strong positive linear trend was also observed between CDOM and *M. polykrikoides* density with 83.3% of the variation in absorbance at 350 nm explained by the density of the bloom.

In the *M. polykrikoides* bloom, SR, a proxy for molecular weight and photodegradability, decreased with increased *M. polykrikoides* density with high SR values at stations 1-3, 7, and 9 and the lowest values at stations 5, 6, 8, and 10 (Figure 5). The SR values, which ranged from 1.16 at station 9 to 0.72 at station 5, indicate that CDOM samples from areas of high densities of *M. polykrikoides* had higher molecular weights and were potentially more photolabile than stations with lower densities of *M. polykrikoides*. The ratio of *a254:a365*, a proxy for molecular weight, ranged from 4.32 at station 8 to 7.57 at station 7, and decreased with increased densities of *M. polykrikoides*, indicating the presence of higher molecular weight CDOM at these stations (Figure 6). Specific UV Absorbance at 254 nm (SUVA$_{254}$), a proxy for CDOM aromaticity, ranged from 0.025 at station 6 to 0.046 at station 7 (Figure 7). SUVA$_{254}$ was lower at higher densities of *M. polykrikoides*, indicating the presence of less aromatic CDOM at these stations. There was good agreement between the optical proxies which suggested that samples from higher bloom densities (stations 5, 6, 8, and 10) had higher molecular weights and lower levels of aromaticity than the stations with lower bloom densities.

A. monilatum Bloom: August 23rd, 2017

A bloom of *A. monilatum* was documented on a cruise on August 23rd, 2017. The cruise sampled stations with bloom densities that ranged from 53 to 175,877 genomes/mL with four sampling stations with cell densities greater than 70,000 genomes/mL (3, 5, 7, and 9) representing the bloom stations. The bloom appeared to increase in density upstream from the mouth of the LYRE. DOC values ranged from 238 at station 1 to 456 µM at station 5 and were

greatest at stations with the greatest densities of *A. monilatum* (Figure 8). Absorbance at 350 nm, at which wavelength CDOM was determined, ranged from 1.89 to 3.80 with the highest values at the stations with the highest densities of *A. monilatum* (stations 5 and 7) (Figure 9). CDOM also appeared to increase upstream from stations 1 to 10. A linear regression model was applied to compare the densities of *A. monilatum* with DOC and CDOM. DOC (Figure 15) and CDOM (Figure 16) were both positively related to densities of *A. monilatum* with bloom density explaining 53.0% of the variation in DOC and 47.8% of the variation in CDOM.

In the August 23rd, 2017 bloom, S_R decreased with increased densities of *A. monilatum* (Figure 10). S_R values ranged from 0.73 at station 5 to 1.06 at station 6. This suggests that the CDOM at stations with greater densities of *A. monilatum* had higher molecular weights and may be more photodegradable than at stations not experiencing blooms. Values of *a254:a365* ranged from 5.38 at station 5 to 7.73 at station 2 with lower values at higher *A. monilatum* densities (Figure 11). Lower *a254:a365* values indicate higher molecular weights suggesting that stations with higher *A. monilatum* densities had higher molecular weight CDOM. SUVA$_{254}$ values ranged from 0.037 at station 6 to 0.051 at station 8 (Figure 12). There appeared to be a weak relationship between SUVA$_{254}$ and *A. monilatum* density with the two stations having the highest SUVA$_{254}$ values (4 and 8) being non-bloom stations and higher *A. monilatum* densities having lower SUVA$_{254}$ values (stations 3, 5 and 7). However, this relationship is much less clear than with the other optical proxies or with the *M. polykrikoides* bloom densities. Overall, the optical proxies demonstrated good agreement, indicating that stations with higher *A. monilatum* densities had higher molecular weights; however, the relationship between aromaticity and *A. monilatum* density was less clear.

Microbial Decomposition Experiments

DOC and DIC

Initial DOC concentrations ranged from 234 µM for the media control to 741 µM for *A. monilatum* with standard deviation values ranging from 8 to 59 µM (Figure 17). A single-factor ANOVA test of the initial values resulted in a p-value of 6.38E-06 indicating that the initial differences among treatments were significant at a confidence level of 95% (Table 1). The final DOC concentrations ranged from 273 µM for the media control to 779 µM for *A. monilatum* with standard deviation values ranging from 6 to 47 µM. The changes in DOC concentration after the 14-day incubation period ranged from -26 µM for *M. polykrikoides* to +39 µM for the media control with high standard deviation values ranging from 12to 43 µM that at times were greater than the actual values. The high standard deviation values are indicative of the substantial variation in response within the different treatments.

The changes in DIC ranged from 165 µM for the media control to 245 µM for *A. monilatum* with standard deviation values ranging from 4 to 209 µM (Figure 19). These differences were confirmed to be significant using a single-factor ANOVA test that gave a p-value of 0.01 which was significant given a 95% confidence interval (Table 4).

To relate the DOC consumed to the DIC produced by the bloom species, given the background concentrations already present in the media, the mean media DOC values were subtracted to remove their impact on the analysis. To account for differences in initial DOC concentrations, the DOC and DIC values were converted to percent change. The percent change in DOC was -0.37 % for *A. monilatum* and -66 % for *M. polykrikoides* (Figure 18). This difference was shown to be significant using a single-factor ANOVA test which resulted in a p-value of 2.94E-04 (Table 3). The percent increase in DIC was 21 % for *A. monilatum* and 33 % for *M. polykrikoides* (Figure 20). This difference was also shown to be significant using a single-

factor ANOVA test which resulted in a p-value of 7.95E-05 (Table 5). These calculations show that differences exist in DOC lability and stimulation of microbial between species as well as between bloom and non-bloom conditions.

CDOM

The initial values for absorbance at 350 nm ranged from a low of 2.28 m^{-1} for the media control to a high of 3.67 m^{-1} for *A. monilatum* with standard deviation values ranging from 0.07 m^{-1} to 0.13 m^{-1} (Figure 21). A single-factor ANOVA test of the initial values resulted in a p-value of 2.73E-12 which indicates that the initial differences among the treatments are significant at a 95% confidence interval (Table 6). The final values ranged from a low of 2.33 m^{-1} for the media control to a high of 3.35 m^{-1} for *A. monilatum* with standard deviations ranging from 0.03 m^{-1} to 0.06 m^{-1}. The media control did not change from intial to final samplings but *A. monilatum* and *M. polykrikoides* had slight decreases in absorbance, suggesting that some CDOM was broken down in the bloom treatments.

Optical Proxies

The initial S_r values ranged from a low of 1.06±01 for CDOM derived from *M. polykrikoides* to a high of 1.41±0.08 for the media control with low standard deviation values between 0.01 and 0.08 (Figure 22). A single-factor ANOVA test of the initial values resulted in a p-value of 1.92E-08 suggests that the initial differences among the treatments are significant given a 95% confidence interval (Table 7). The final values ranged from 0.98 for *M. polykrikoides* derived CDOM to a high of 1.32 for the media control with low standard deviation ranging from 0.01 to 0.02. The S_R values of CDOM derived from *M. polykrikoides* and the media control both decreased during incubation while S_R for *A. monilatum* remained constant. These

results suggest that the bloom samples had CDOM with higher molecular weights and higher degrees of photodegradability than the media control.

The initial *a254:a365* values ranged from a low of 7.14 for *A. monilatum* derived CDOM to a high of 7.92 for the media control with standard deviations ranging from 0.12 to 0.30 (Figure 23). A single-factor ANOVA test of the initial values resulted in a p-value of 8.18E-05, which indicates that the initial differences among the treatments were significant at a 95% confidence interval (Table 8). The final values ranged from 7.69 for the media control to 7.92 for *M. polyrikoides* derived CDOM with standard deviation values ranging from 0.03 to 0.30. The *a254:a365* values for *A. monilatum* and *M. polykrikoides* increased over the incubation period while the values for the media control decreased. This suggests that in the bloom treatments higher molecular weight CDOM was preferentially broken down over the course of the incubation, whereas in the media control lower molecular weight CDOM was preferentially broken down over the course of the incubation.

The intial $SUVA_{254}$ values ranged from 0.0256 for *A. monilatum* to a high of 0.0566 for the media control with standard deviations ranging between 0.0010 and 0.0017 (Figure 24). A single-factor ANOVA test of the initial values resulted in a p-value of 1.81E-06 which indicates that the initial differences among the treatments were significant at a 95% confidence interval (Table 9). The final values ranged from 0.0238 for *A. monilatum* to a high of 0.0487 for the media control with standard deviations ranging from 0.0010 to 0.0046. There appeared to be little change between the initial and final values for *A. monilatum* and *M. polykrikoides* while the media appeared to decrease slightly. This indicates that the two bloom species treatments had CDOM pools with lower average aromaticity levels than the media control.

Sediment Core Incubations

The initial DOC values for *M. polykrikoides* and both controls were close in value,

469±28 µM for control 1 and 522±62 µM for *M. polykrikoides*. The *A. monilatum* DOC

concentration was much larger at 1586±150 µM (Figure 25). During incubations, the DOC

concentrations were reduced for *M. polykrikoides* and the two controls, ranging from -76±57 µM

for *M. polykrikoides* to -92±32 µM for control 1 (Figure 27). The *A. monilatum* treatment

experienced a decrease in DOC concentration of -292±104 µM. The changes in DOC were

shown to be significantly different given a 95% confidence interval using a single-factor

ANOVA test which resulted in a p-value of 0.0071.

The change in DIC values were similar across treatments, ranging from +66±8 µM for

control 1 to 113±43 µM for control 2 (Figures 26 and 27). These similarities were confirmed

using a single-factor ANOVA test which had a p-value of 0.69, indicating the changes in DIC

concentration were not significantly different according to a 95% confidence interval.

Discussion

Impact of HABs on the DOC Pool

Both *A. monilatum* and *M. polykrikoides* increased the size of the DOC and CDOM

pools. The *in situ* measurements from August 2017 deomonstrated clear trends where higher

concentrations of DOC and CDOM were present in bloom patches with higher densities of *M.*

polykrikoides (Figures 3 and 4) and *A. monilatum* (Figures 8 and 9). These visual trends were

confirmed with linear regression models, which all showed positive linear correlations between

bloom species density, DOC concentration, and absorbance at 350 nm. This trend was especially

clear in the *M. polykrikoides* bloom with over 80% of the variation in DOC and CDOM could be

explained by cell density of *M. polykrikoides* and approximately 50% of the variation explained

by cell density for *A. monilatum*. This may be the result of differences in DOC and CDOM

production between the species or it may reflect increased terrestrial signal or grazing during the

A. monilatum bloom, particularly for the CDOM values. Figure 9 shows increases in absorbance

along the upstream gradient which may be reflective of increased levels of highly-aromatic,

terrestrially-produced, allochthonous CDOM which would be diluted by mixing with water from

the Chesapeake Bay further downstream. $SUVA_{254}$, a proxy for aromaticity, also showed an

increase along the upstream gradient, supporting this interpretation. However, it has also been

shown that some HAB species in mid-Atlantic estuaries are mixotrophic which allows them to

utilize autotrophic and heterotrophic metabolism (Mulholland et al. 2018). That could be the case

with *A. monilatum* and *M. polykrikoides* which could also be consuming DOC as part of their

carbon supply to either initiate their blooms or as a secondary source once self-shading reduces

the efficiency of primary productivity. If *A. monilatum* is utilizing DOC as a source of carbon,

that would explain the reduced relationship with DOC in the linear regression compared with *M.*

polykrikoides.

    A. monilatum and *M. polykrikoides* also increased the concentrations of DOC and CDOM

in culture. Even at cell counts much lower than bloom conditions (approximately 9,000 for *A.*

monilatum and 2,200 for *M. polykrikoides*), the initial DOC concentrations and CDOM

measurements were significantly greater than in the media control (Figures 17 and 21, Tables 3

and 6). The good agreement between the *in situ* field samples and the laboratory culture samples

supports the interpretation that HAB species increase the size of the DOC pool in estuaries. This

result is not surprising as phytoplankton have frequently been documented to be sources of DOC

and CDOM to marine systems (Carlson and Hansell 2015). Intense blooms in particular have

been shown to result in accumulation of DOC and CDOM as the production rate of organic carbon outpaces its respiration (Suksomjit et al. 2009). It is worth noting that the blooms led to significant, measurable increases in the CDOM pool as normally CDOM is considered a tracer of terrestrial input in estuaries: a finding that should be taken into consideration as CDOM is increasingly used as an easy, efficient tool to measure DOC in estuaries (Canuel et al. 2012).

In addition to impacting the quantity of the DOC pool, *A. monilatum* and *M. polykrikoides* were also shown to alter the composition of the DOC pool. In the *in situ* samples, both HAB species decreased the slope ratio, the ratio of 254:356, and the $SUVA_{254}$ value (Figures 5-7, 10-12). These differences translate into a CDOM pool that has a higher average molecular weight, a higher degree of photodegradability, and lower level of aromaticity than the background CDOM pool. These changes to the CDOM pool were also reflected in the laboratory studies where the *A. monilatum* and *M. polykrikoides* cultures produced CDOM that had a significantly higher average molecular weight and a significantly lower average level of aromaticity than the media control (Figures 22-24). These results differ from common understandings of CDOM composition where terrestrial CDOM is high in molecular weight and aromaticity, while marine phytoplankton produce CDOM that has a lower molecular weight and lower level of aromaticity (Romera-Catillo et al. 2010, Leech et al. 2016). However, these studies were conducted to examine geographic or seasonal differences and did not focus on intense algal blooms. Additionally, it has been documented that intense blooms can result in the accumulation of humic substances (Sukomjit et al. 2009). Bloom conditions are large perturbations to the system, and the massive increase in the DOC and CDOM pools may allow for the accumulation of phytoplankton produced CDOM that would otherwise be rapidly respired or broken down in standard conditions, confounding the CDOM signature of phytoplankton in

these earlier studies. One implication of blooms producing significant quantities of CDOM is that CDOM can absorb light, shading phototrophic species lower in the water column and in the benthos, reducing their ability to photosynthesize. Another implication is that CDOM is highly photodegradable, providing an alternative, abiotic removal mechanism that must be accounted for in carbon budgets (Helms et al. 2014). The combined data from the laboratory cultures and *in situ* measurements confirm that blooms substantially alter the quantity and quality of the DOC pool, supporting H1.

Microbial Decomposition

Microbial respiration was significantly increased by the bloom species suggesting that the blooms increased the decomposition of DOC by pelagic microbes, supporting H2 where it was predicted that the blooms would stimulate pelagic microbial respiration (Figure 18). Furthermore, decreases in the concentration of DOC and CDOM produced by *A. monilatum* and *M. polykrikoides* were noted in the microbial incubation experiments (Figures 17, 18, and 21). Changes in the character of the CDOM pool over the course of the incubations were also documented. In the *A. monilatum* and *M. polykrikoides* treatments, the *a254:a365* ratio increased, indicating that the average molecular weight decreased. A decrease in CDOM molecular weight suggests that the higher molecular weight CDOM produced during the bloom was preferentially respired compared to non-bloom produced CDOM (Figure 23). The stimulation of pelagic microbial metabolism by increased DOC inputs from phytoplankton have been previously documented, but the optical signatures from incubations focusing on alterations of CDOM pools have typically shown the preferential consumption of lower molecular weight CDOM leading to lower SR or *a254:a365* signatures (Lake et al. 2013, Helms et al 2008). However, the incubations in the other studies have been conducted with environmental water

samples from non-bloom conditions and the highly-labile, phytoplankton-produced CDOM may have already been decomposed.

There also appeared to be species level differences in the character of the DOC contributions of *A. monilatum* and *M. polykrikoides*. The DOC and CDOM produced by *M. polykrikoides* were substantially more labile than the DOC and CDOM produced by *A. monilatum*. These differences were evident both in the percent decrease in DOC but also in the percent increases in DIC, indicating increased respiration (Figures 18 and 20). Species-level differences in bloom-produced DOC and CDOM have been documented in other studies and these results indicate that the differences in these DOC contributions result in different levels of lability to pelagic microbes (Shuksomjit et al. 2009, Romera-Catillo et al. 2010). This suggests that the DOC produced by different species of phytoplankton cannot be treated exactly the same for metabolic calculations used in models to predict the impact of nutrient loads and climate change on hypoxia (Lake and Brush 2015). Additionally, these species-specific differences between *A. monilatum* and *M. polykrikoides* suggest that monitoring efforts using CDOM sensing or remote sensing efforts should attempt to account for these differences in the character of the CDOM produced by various bloom organisms.

Benthic Metabolism

The key finding from the sediment core incubations was that there was little impact by the blooms on benthic microbial metabolism on short timescales, which did not support H3 which suggested that the blooms would stimulate benthic respiration (Figure 27). Stimulation of benthic respiration has been proposed as an important process in the impact of HABs on estuarine carbon cycling, but this experiment did not support this hypothesis. There were no differences in DIC produced during incubations of the control, *M. polykrikoides*, and *A.*

monilatum. There was a significantly greater loss of DOC in incubations of *A. monilatum* compared to the other three treatments. Given that the changes in DIC and DOC were roughly equal for *M. polykrikoides* and the controls, it is assumed that benthic respiration accounted for the decrease in DOC in these treatments. However, respiration was not able to fully explain the decrease in DOC for the *A. monilatum* treatment, suggesting that another removal process was likely at work. A potential mechanism for enhanced DOC removal in this treatment is sorption onto sinking particulate organic carbon. This process has been documented in ocean systems and the large quantities of sinking particulates produced by HABs would allow this process to occur on a measurable scale (Hansell and Carlson 2014).

Conclusions and Future Directions

This study documented the impact of two HAB species, *A. monilatum* and *M. polykrikoides* on the DOC pool and microbial respiration in the LYRE. The bloom species were shown to greatly increase the quantity and alter the quality of the DOC and CDOM pools in the estuary. The blooms were shown to stimulate pelagic microbial respiration by providing labile DOC and CDOM that were preferentially respired compared to other DOC in the water column. Additionally, these experiments highlighted the species-specific differences of phytoplankton produced DOC, with *M. polykrikoides* producing more labile DOC than *A. monilatum*. The increased DOC did not stimulate benthic metabolism on short timescales. However, the sediment core experiments highlighted another potential DOC removal mechanism during blooms: sorption to sinking particulate matter. This study paves the way for future work in examining the differences in phytoplankton contributions to the DOC pool, characterization of sorption to POC as a removal mechanism for DOC in estuaries, and improving monitoring efforts through improved understanding of how *A. monilatum* and *M. polykrikoides* impact CDOM signatures.

References:

Anderson, I. C., Brush, M. J., Piehler, M. F., Currin, C. A., Stanhope, J. W., Smyth, A. R., ... & Whitehead, M. L. (2014). Impacts of climate-related drivers on the benthic nutrient filter in a shallow photic estuary. *Estuaries and coasts*, 37(1), 46-62.

Bauer, J. E., Cai, W. J., Raymond, P. A., Bianchi, T. S., Hopkinson, C. S., & Regnier, P. A. (2013). The changing carbon cycle of the coastal ocean. *Nature*, 504(7478), 61.

Canuel, E. A., Cammer, S. S., McIntosh, H. A., & Pondell, C. R. (2012). Climate change impacts on the organic carbon cycle at the land-ocean interface. *Annual Review of Earth and Planetary Sciences*, 40, 685-711.

Castillo, C. R., Sarmento, H., Alvarez-Salgado, X. A., Gasol, J. M., & Marraséa, C. (2010). Production of chromophoric dissolved organic matter by marine phytoplankton. *Limnology and Oceanography*, 55(1), 446-454.

Crosswell, J. R., Anderson, I. C., Stanhope, J. W., Van Dam, B., Brush, M. J., Ensign, S., ... & Paerl, H. W. (2017). Carbon budget of a shallow, lagoonal estuary: Transformations and source-sink dynamics along the river-estuary-ocean continuum. *Limnology and Oceanography*, 62(S1), S29-S45.

De Haan, H., & De Boer, T. (1987). Applicability of light absorbance and fluorescence as measures of concentration and molecular size of dissolved organic carbon in humic Lake Tjeukemeer. *Water research*, 21(6), 731-734.

Hansell, D. A., & Carlson, C. A. (Eds.). (2014). Biogeochemistry of marine dissolved organic matter. *Academic Press*.

Harding, J. M., Mann, R., Moeller, P., & Hsia, M. S. (2009). Mortality of the veined rapa whelk, Rapana venosa, in relation to a bloom of Alexandrium monilatum in the York River, United States. *Journal of Shellfish Research*, 28(2), 363-368.

Heisler, J., Glibert, P. M., Burkholder, J. M., Anderson, D. M., Cochlan, W., Dennison, W. C., ... & Lewitus, A. (2008). Eutrophication and harmful algal blooms: a scientific consensus. *Harmful algae*, 8(1), 3-13.

Helms, J. R., Mao, J., Stubbins, A., Schmidt-Rohr, K., Spencer, R. G., Hernes, P. J., & Mopper, K. (2014). Loss of optical and molecular indicators of terrigenous dissolved organic matter during long-term photobleaching. *Aquatic sciences*, 76(3), 353-373.

Helms, J. R., Stubbins, A., Ritchie, J. D., Minor, E. C., Kieber, D. J., & Mopper, K. (2008). Absorption spectral slopes and slope ratios as indicators of molecular weight, source, and photobleaching of chromophoric dissolved organic matter. Limnology and *Oceanography*, 53(3), 955-969.

Lake, S. J., & Brush, M. J. (2015). Contribution of nutrient and organic matter sources to the development of periodic hypoxia in a tributary estuary. *Estuaries and coasts*, 38(6), 2149-2171.

Lake, S. J., Brush, M. J., Anderson, I. C., & Kator, H. I. (2013). Internal versus external drivers of periodic hypoxia in a coastal plain tributary estuary: the York River, Virginia. *Marine Ecology Progress Series*, 492, 21-39.

Marshall, H. G., & Egerton, T. A. (2009, October). Increasing occurrence and development of potentially harmful algal blooms in Virginia tidal rivers. In *Conference Proceedings: Water Resources in Changing Climates*. Virginia Tech Virginia Water Research Center, October, Richmond, VA (pp. 89-101).

McGlathery, K. J., Anderson, I. C., & Tyler, A. C. (2001). Magnitude and variability of benthic and pelagic metabolism in a temperate coastal lagoon. *Marine ecology progress series*, 216, 1-15.

Mulholland, M. R., Morse, R., Egerton, T., Bernhardt, P. W., & Filippino, K. C. (2018). Blooms of dinoflagellate mixotrophs in a lower Chesapeake Bay tributary: carbon and nitrogen uptake over diurnal, seasonal, and interannual timescales. *Estuaries and coasts*, 1-22.

Murphy, A. E., Nizzoli, D., Bartoli, M., Smyth, A. R., Castaldelli, G., & Anderson, I. C. (2018). Variation in benthic metabolism and nitrogen cycling across clam aquaculture sites. *Marine pollution bulletin*, 127, 524-535.

Neubauer, S. C., & Anderson, I. C. (2003). Transport of dissolved inorganic carbon from a tidal freshwater marsh to the York River estuary. *Limnology and Oceanography*, 48(1), 299-307.

Shen, J., & Haas, L. (2004). Calculating age and residence time in the tidal York River using three-dimensional model experiments. Estuarine, *Coastal and Shelf Science*, 61(3), 449-461.

Suksomjit, M., Nagao, S., Ichimi, K., Yamada, T., & Tada, K. (2009). Variation of dissolved organic matter and fluorescence characteristics before, during and after phytoplankton bloom. *Journal of Oceanography*, 65(6), 835-846.

Vähätalo, A. V., & Wetzel, R. G. (2004). Photochemical and microbial decomposition of chromophoric dissolved organic matter during long (months–years) exposures. *Marine Chemistry*, 89(1-4), 313-326.

Van Dam, B. R., Crosswell, J. R., Anderson, I. C., & Paerl, H. W. (2018). Watershed-Scale Drivers of Air-Water CO2 Exchanges in Two Lagoonal North Carolina (USA) Estuaries. *Journal of Geophysical Research: Biogeosciences*, 123(1), 271-287.

Weishaar, J. L., Aiken, G. R., Bergamaschi, B. A., Fram, M. S., Fujii, R., & Mopper, K. (2003). Evaluation of specific ultraviolet absorbance as an indicator of the chemical composition and reactivity of dissolved organic carbon. *Environmental science & technology*, 37(20), 4702-4708.

Wiegner, T. N., & Seitzinger, S. P. (2004). Seasonal bioavailability of dissolved organic carbon and nitrogen from pristine and polluted freshwater wetlands. *Limnology and Oceanography*, 49(5), 1703-1712.

Yamashita, Y., Maie, N., Briceño, H., & Jaffé, R. (2010). Optical characterization of dissolved organic matter in tropical rivers of the Guayana Shield, Venezuela. *Journal of Geophysical Research: Biogeosciences*, 115(G1).

Tables and Figures:

Figure 1: Map of the Lower York River Estuary (LYRE) with the collection location for sediment cores marked with a star.
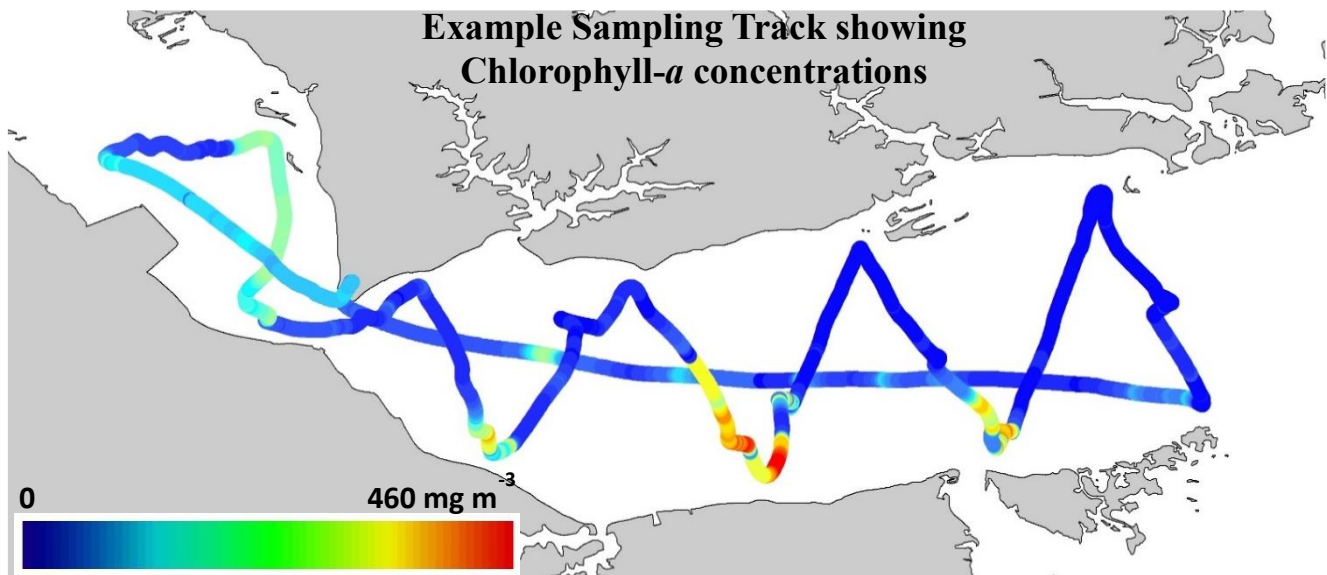
Figure 2: Example cruise track highlighting chlorophyll-*a* densities in the LYRE. Samples were collected from stations within and outside of these high chlorophyll-a density regions for the *in situ* sampling. The specific location of sampling stations changed during each cruise as the blooms changed position in the estuary.
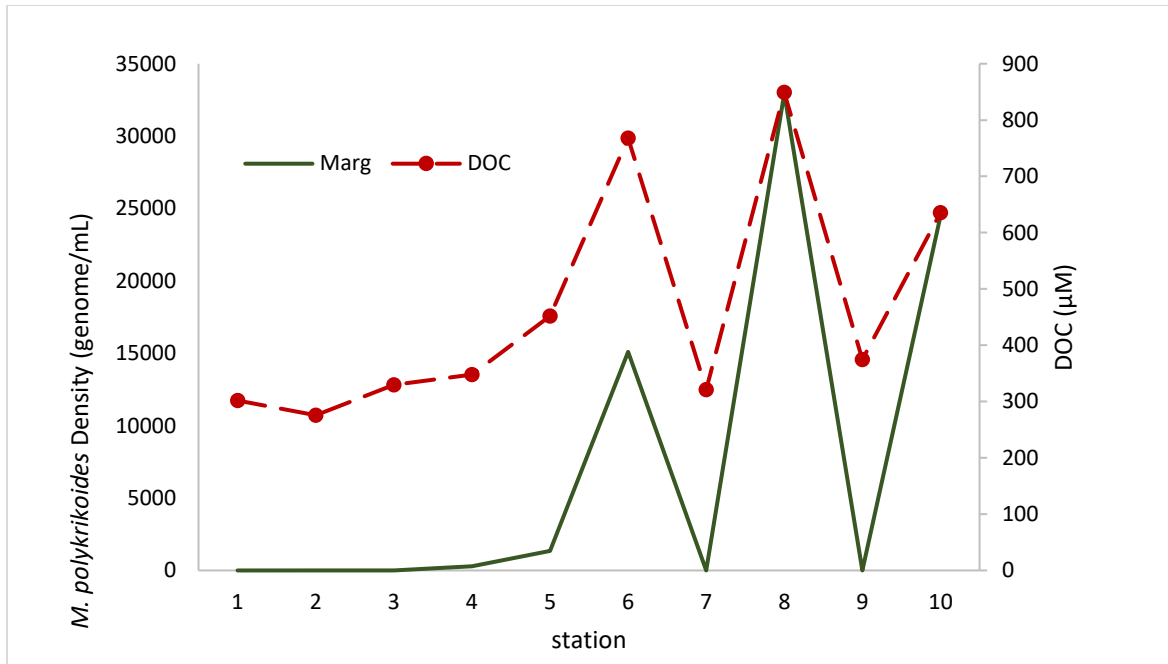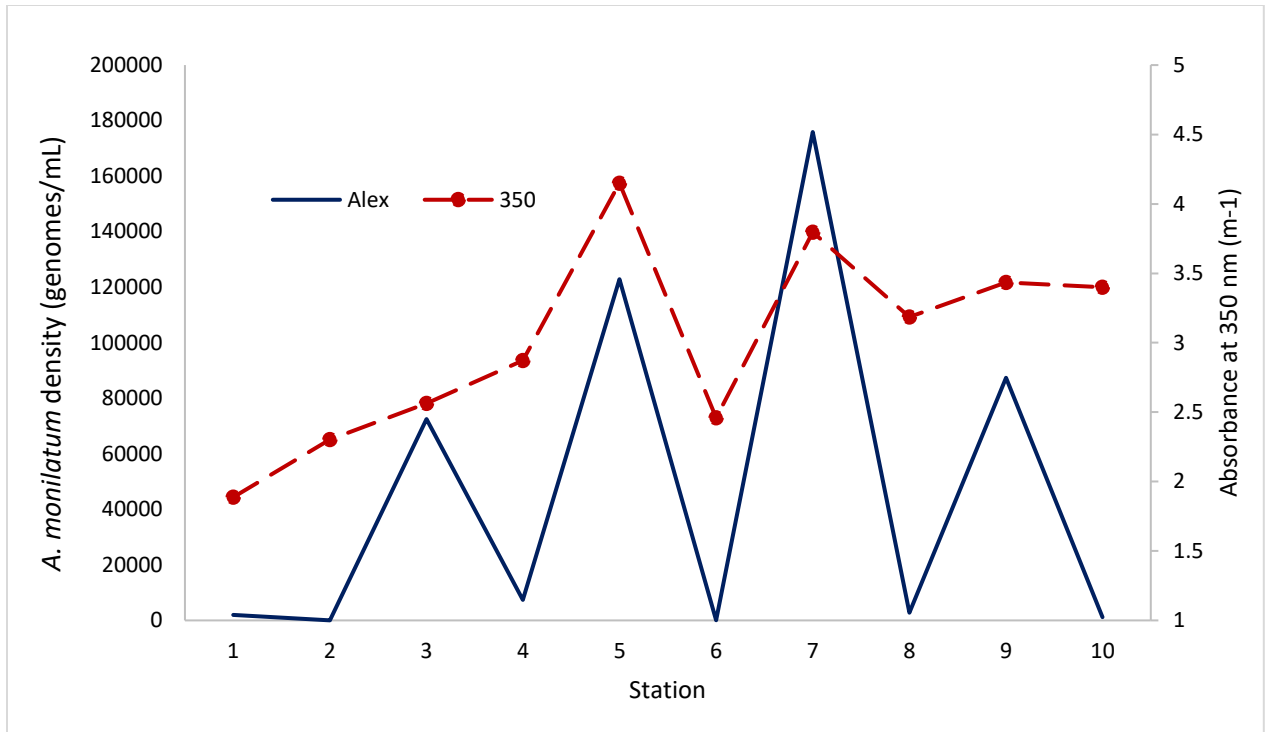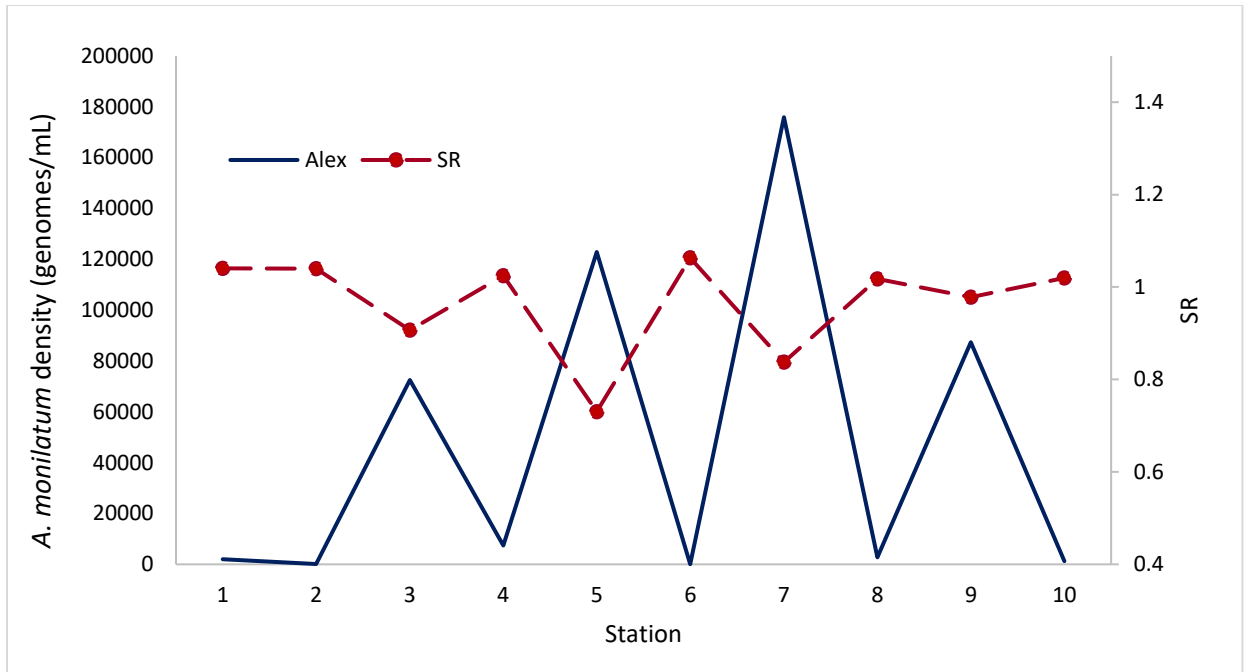
Figure 3: *In situ* samples of DOC [μM] and *M. polykrikoides* density [genome/mL] at stations in and out of the blooms moving up the York River during an *M. polykrikoides* bloom on August 9th, 2017.
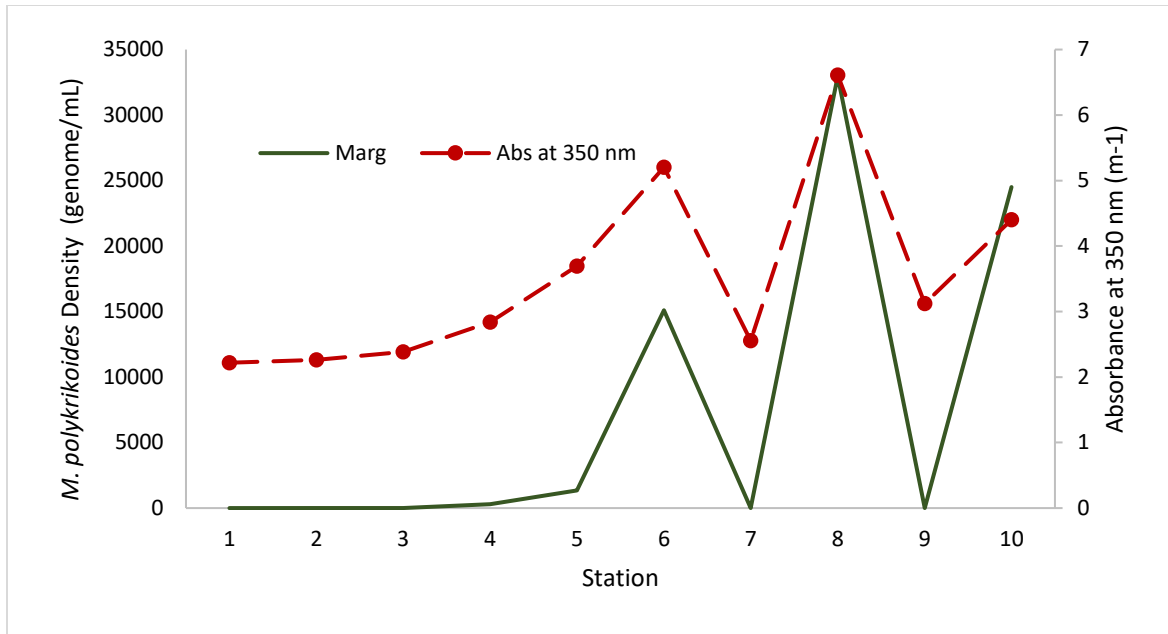
Figure 4: *In situ* samples of CDOM (measured as Absorbance at 350 nm) and *M. polykrikoides* density [genome/mL] at stations in and out of the blooms moving up the York River during an *M. polykrikoides* bloom on August 9th, 2017.
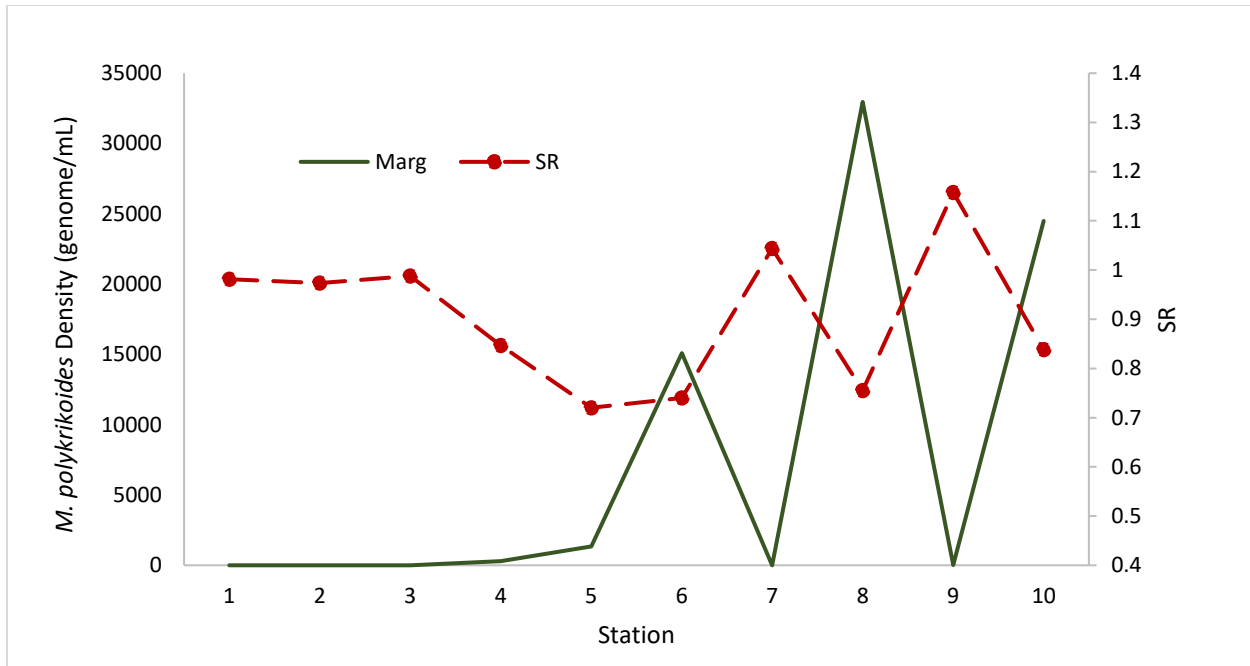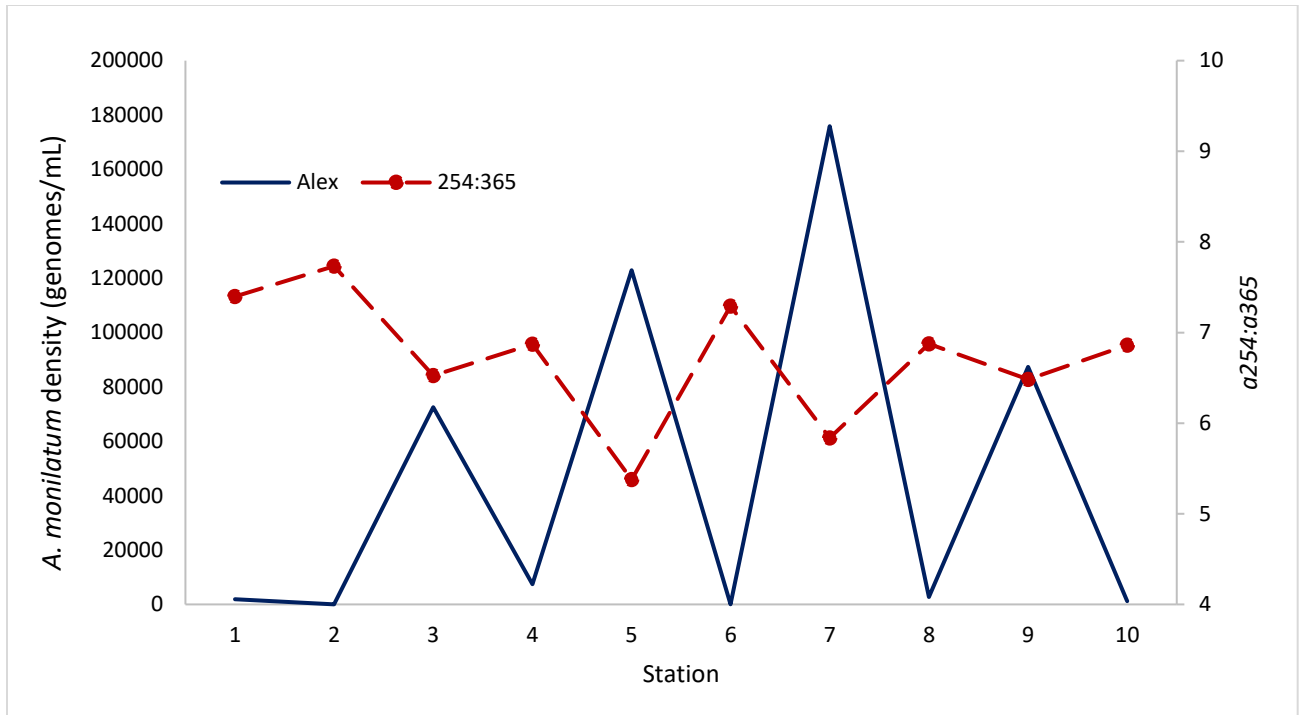
Figure 5: *In situ* samples of SR and *M. polykrikoides* density [genome/mL] at stations in and out of the blooms moving up the York River during an *M. polykrikoides* bloom on August 9th, 2017.
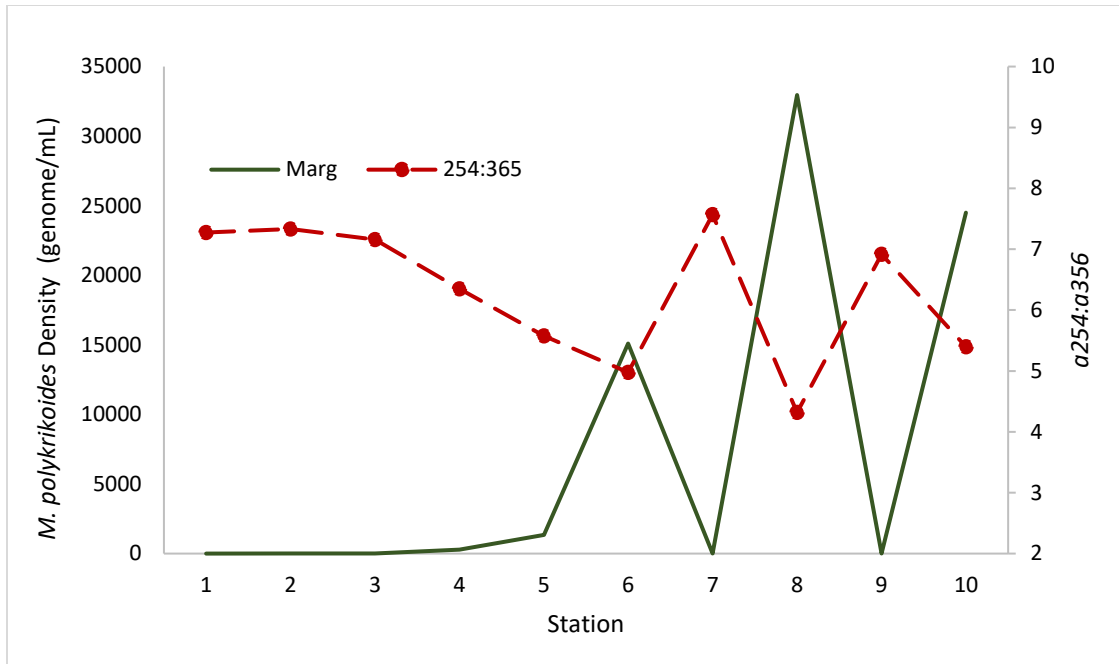
Figure 6: *In situ* samples of *a254:a365* values for *M. polykrikoides* density [genome/mL] at stations in and out of the blooms moving up the York River during an *M. polykrikoides* bloom on August 9th, 2017.
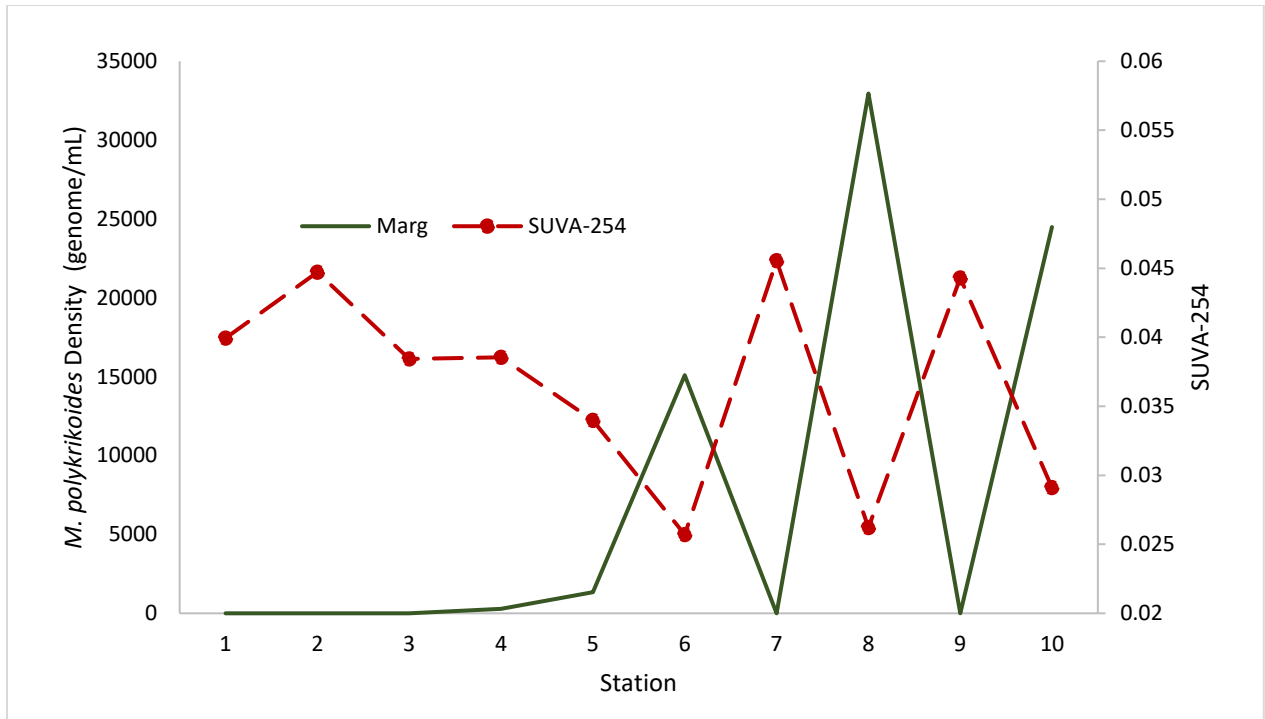
Figure 7: *In situ* samples of SUVA$_{254}$ values for *M. polykrikoides* density [genome/mL] at stations in and out of the blooms moving up the York River during an *M. polykrikoides* bloom on August 9th, 2017.
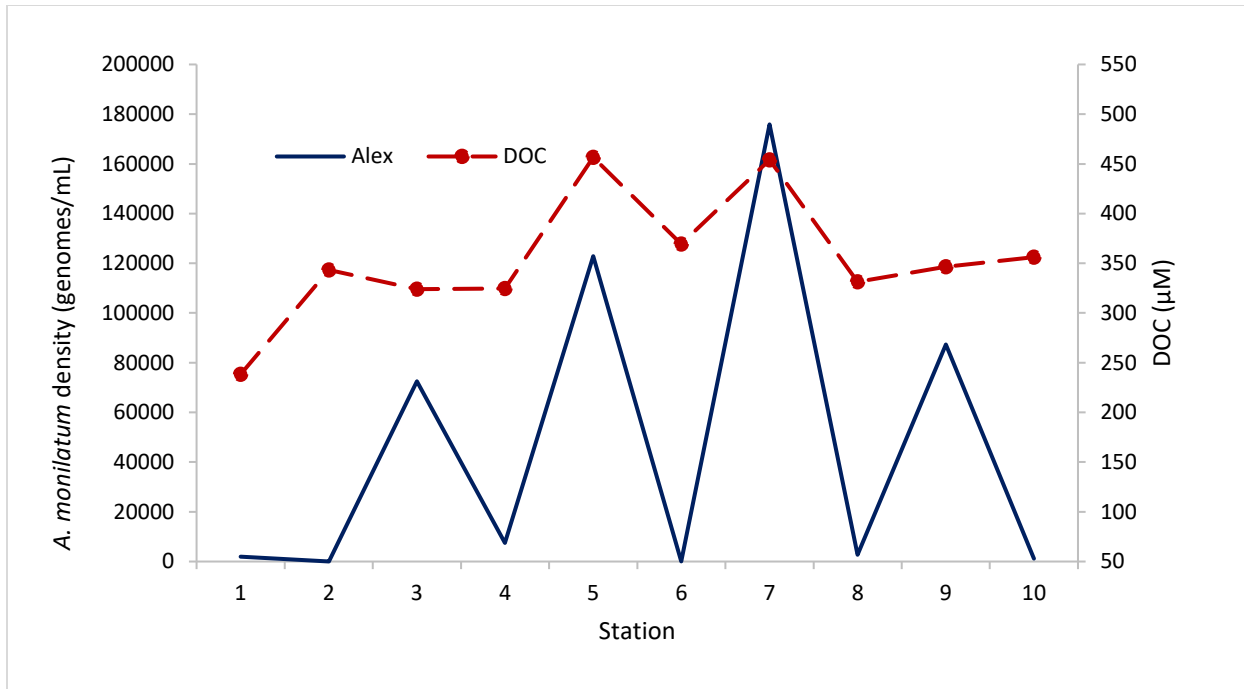
Figure 8: *In situ* samples of DOC [µM] and *A. monilatum* density [genome/mL] at stations in and out of the blooms moving up the York River during an *A. monilatum* bloom on August 23th, 2017.
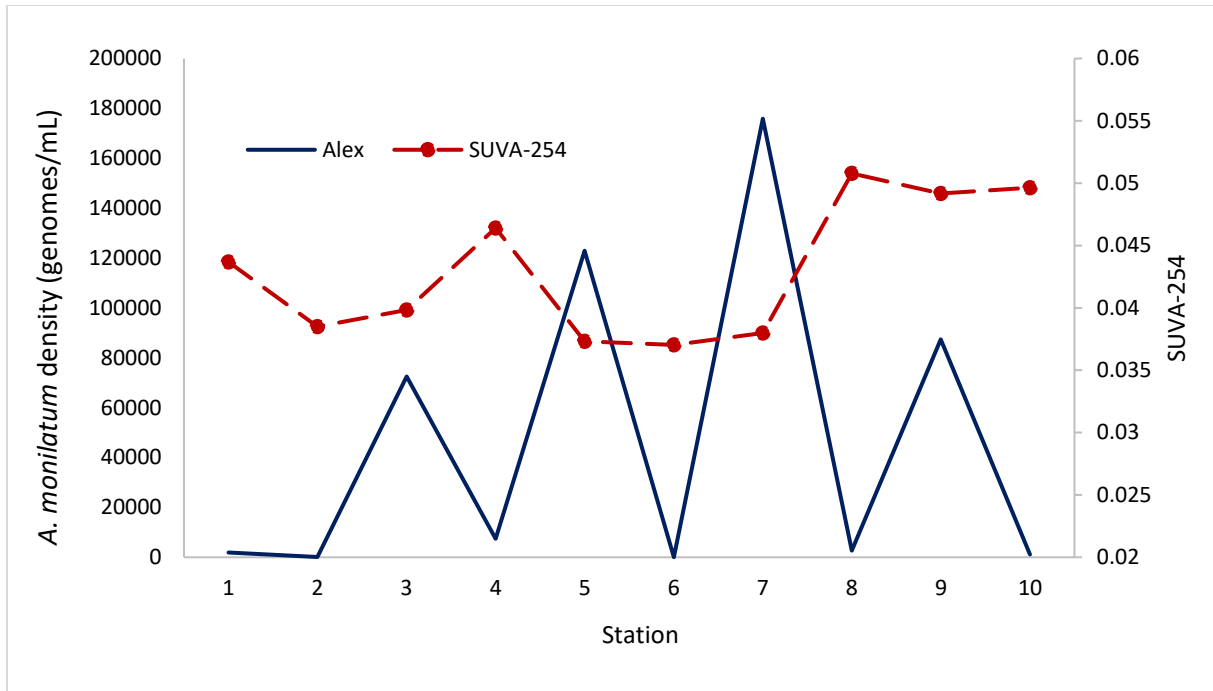
Figure 9: *In situ* samples of Absorbance at 350 nm and *A. monilatum* density [genome/mL] at stations in and out of the blooms moving up the York River during an *A. monilatum* bloom on August 23th, 2017.

Figure 10: *In situ* samples of slope ratio and *A. monilatum* density [genome/mL] at stations in and out of the blooms moving up the York River during an *A. monilatum* bloom on August 23th, 2017.

Figure 11: *In situ* samples of *a254:a365* and *A. monilatum* density [genome/mL] at stations in and out of the blooms moving up the York River during an *A. monilatum* bloom on August 23th, 2017.

Figure 12: In-situ samples of SUAV$_{254}$ and *A. monilatum* density [genome/mL] at stations in and out of the blooms moving up the York River during an *A. monilatum* bloom on August 23th, 2017.
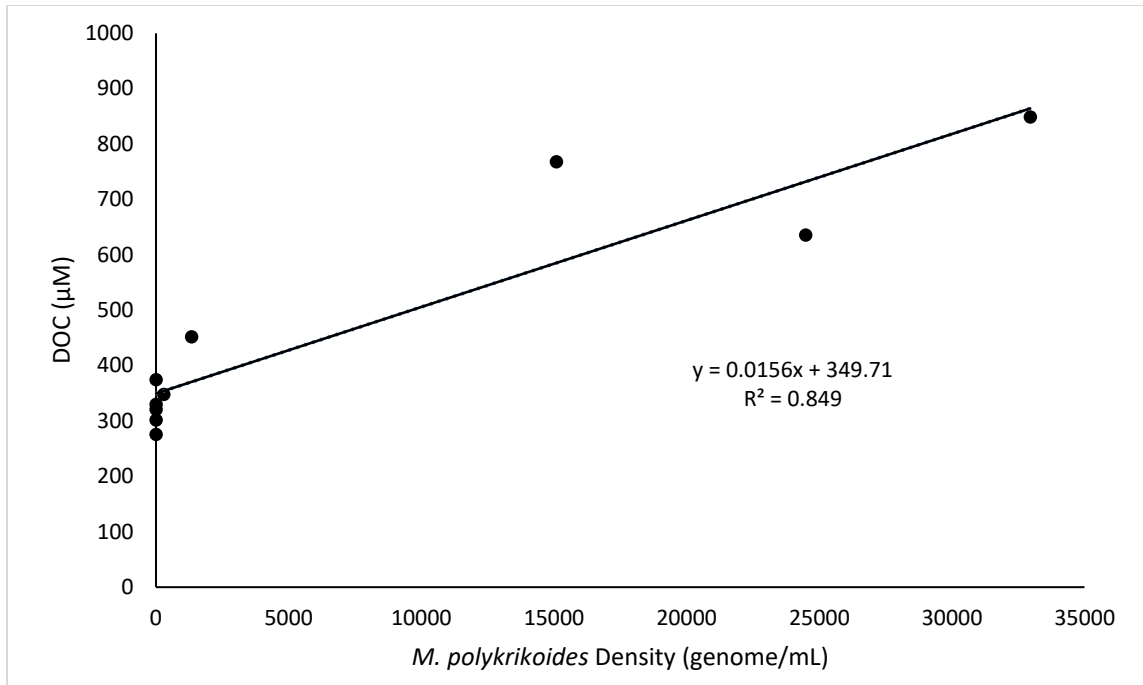
Figure 13: Linear regression of *M. polykrikoides* density vs. DOC concentration for the August 9th, 2017 bloom
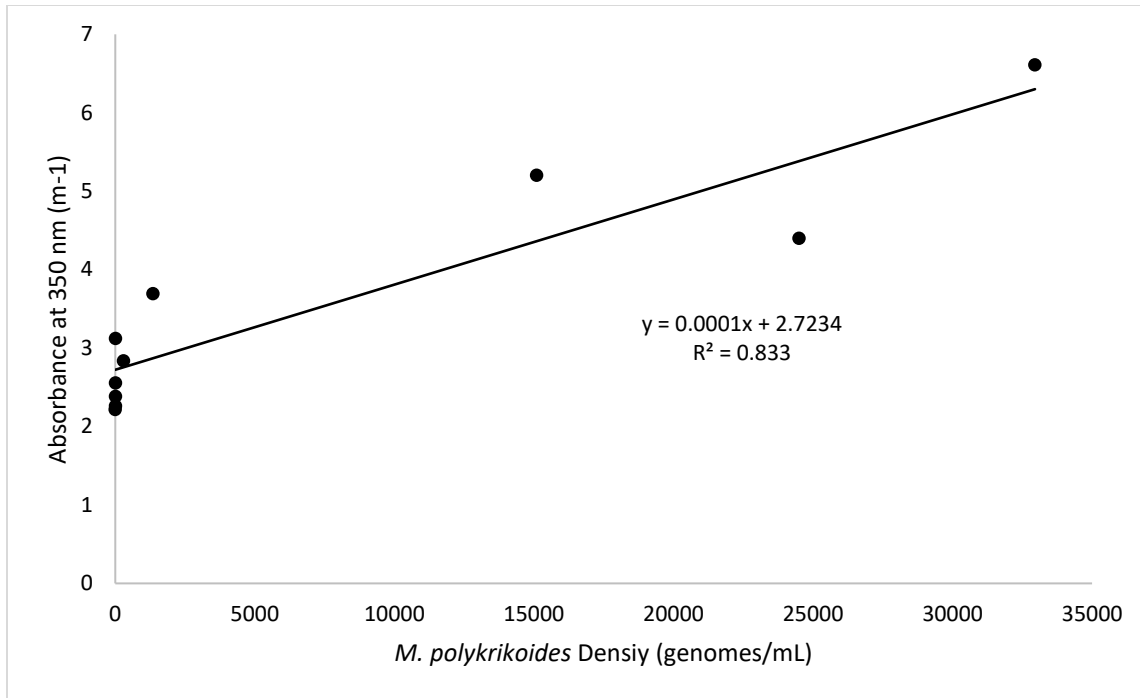
Figure 14: Linear regression of *M. polykrikoides* density vs Absorbance at 350 nm for August 9th, 2017 bloom
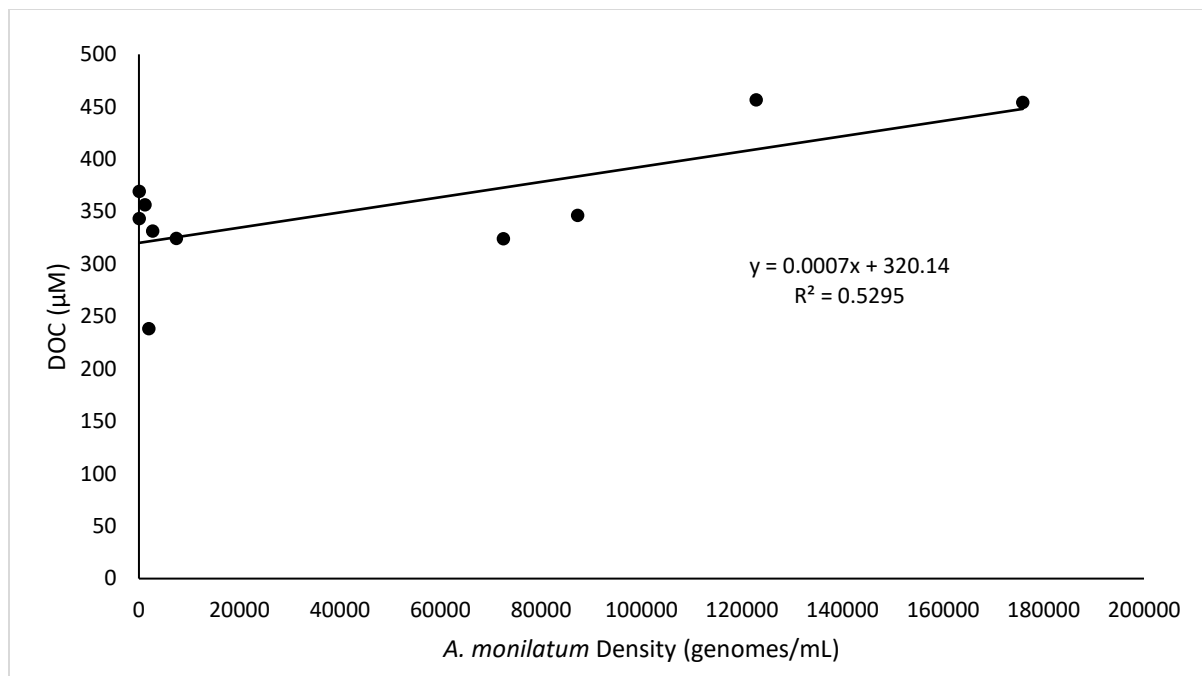
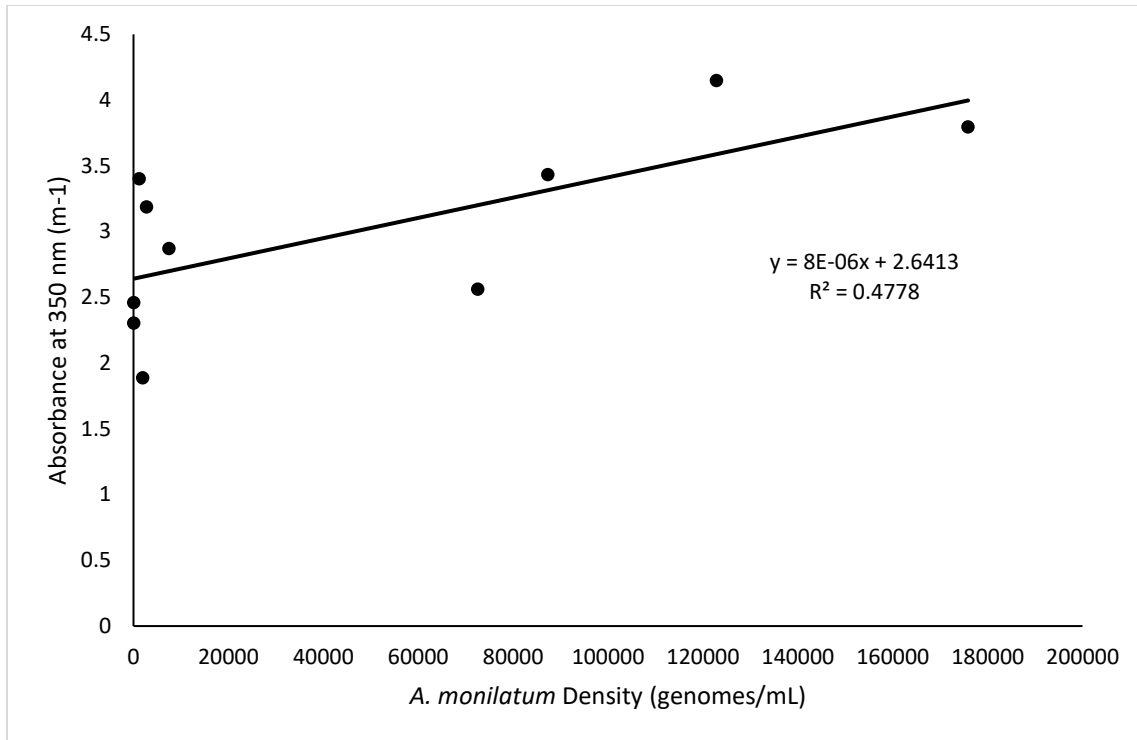Figure 15: Linear regression of *A. monilatum* density vs DOC concentration for August 23rd, 2017 bloom

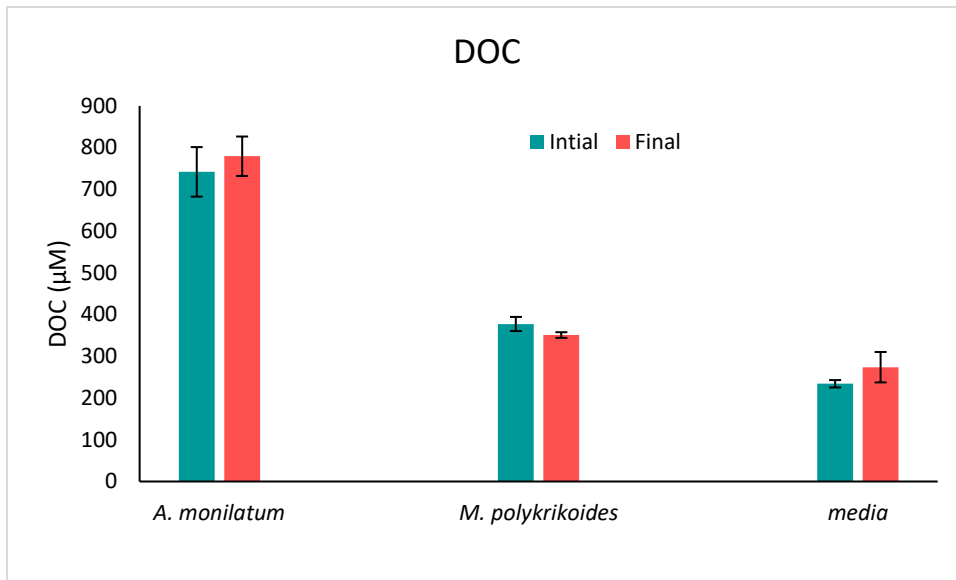Figure 16: Linear regression of *A. monilatum* density vs Absorbance at 350 nm for August 23rd, 2017 bloom

Figure 17: Comparison of initial and final DOC concentrations from the microbial decomposition experiments. Error bars show one standard deviation.

ANOVA						
Source of Variation	*SS*	*df*	*MS*	*F*	*P-value*	*F crit*
Between Groups	411205.5	2	205602.8	158.7843	6.38E-06	5.143253
Within Groups	7769.136	6	1294.856			
Total	418974.7	8				

Table 1: Single-factor ANOVA test of initial DOC concentrations for the microbial decomposition experiment

ANOVA						
Source of Variation	*SS*	*df*	*MS*	*F*	*P-value*	*F crit*
Between Groups	8467.457	2	4233.729	5.795361	0.039683	5.143253
Within Groups	4383.225	6	730.5375			
Total	12850.68	8				

Table 2: Single-factor ANOVA test comparing the change in DOC concentrations from initial to final for the microbial decomposition experiment
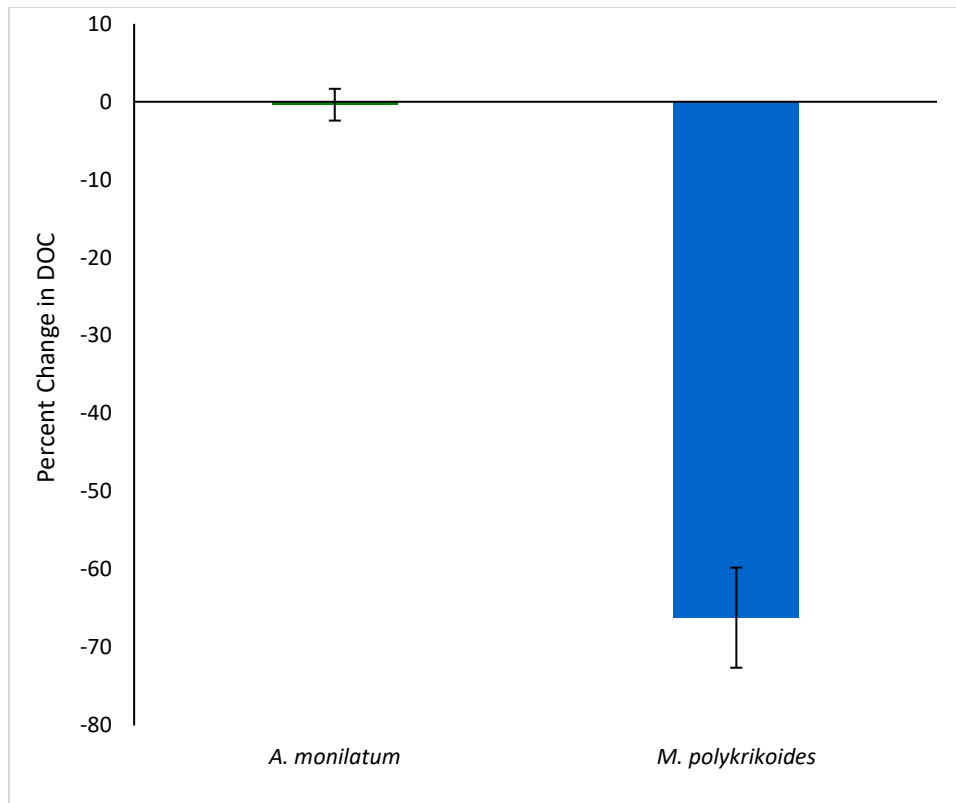
Figure 18: Comparison of the percent change in the concentration of DOC attributed to *A. monilatum* and the concentration of DOC attributed to *M. polykrikoides*. Error bars represent one standard deviation.

ANOVA						
Source of Variation	*SS*	*df*	*MS*	*F*	*P-value*	*F crit*
Between Groups	4752.05	1	4752.05	139.5727	0.000294	7.708647
Within Groups	136.1886	4	34.04714			
Total	4888.239	5				

Table 3: Single Factor ANOVA comparing the percent change in DOC concentration attributed to *A. monilatum* and *M. polykrikoides*.
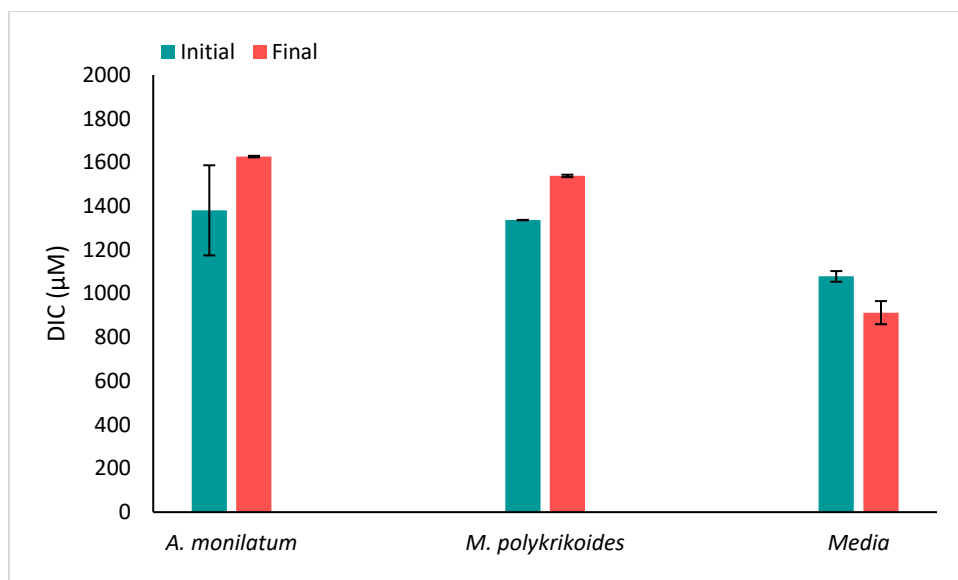
Figure 19: Comparison of initial and final DIC concentrations from the microbial decomposition experiments. Error bars show one standard deviation.

ANOVA						
Source of Variation	*SS*	*df*	*MS*	*F*	*P-value*	*F crit*
Between Groups	306714.8	2	153357.4	10.27313	0.011546	5.143253
Within Groups	89568.04	6	14928.01			
Total	396282.8	8				

Table 4: Single-factor ANOVA test comparing the changes from initial to final DIC values for the microbial decomposition experiments
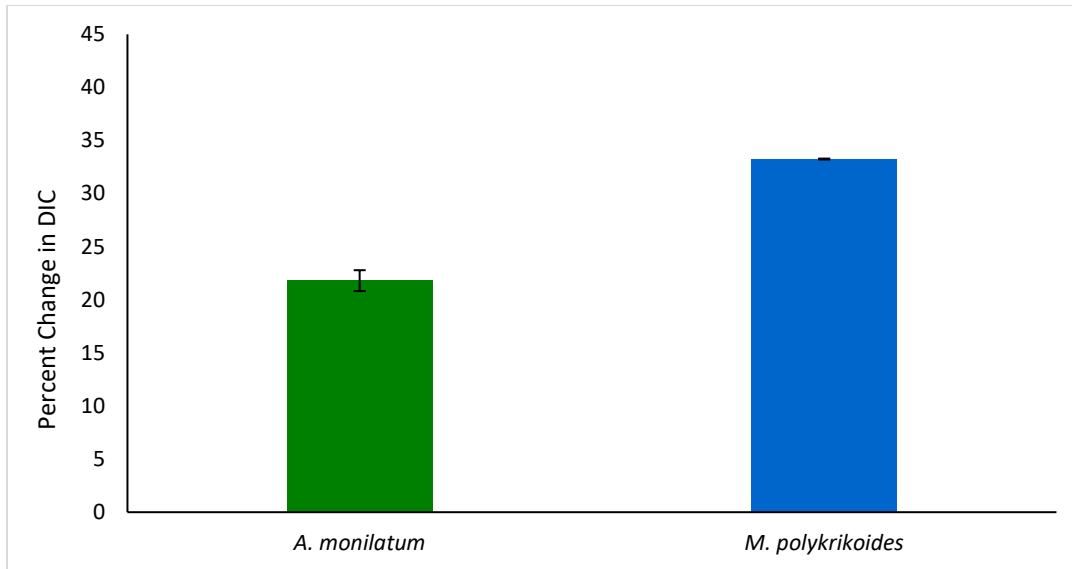
Figure 20: Comparison of the percent change in DIC attributed to *A. monilatum* and *M. polykrikoides* from initial to final for the microbial decomposition experiments. Error bars show one standard deviation.

ANOVA						
Source of Variation	*SS*	*df*	*MS*	*F*	*P-value*	*F crit*
Between Groups	196.6434	1	196.6434	271.3272	7.95E-05	7.708647
Within Groups	2.898985	4	0.724746			
Total	199.5424	5				

Table 5: Single Factor ANOVA test comparing the percent change in DIC of *A. monilatum* and *M. polykrikoides* corrected for the control.
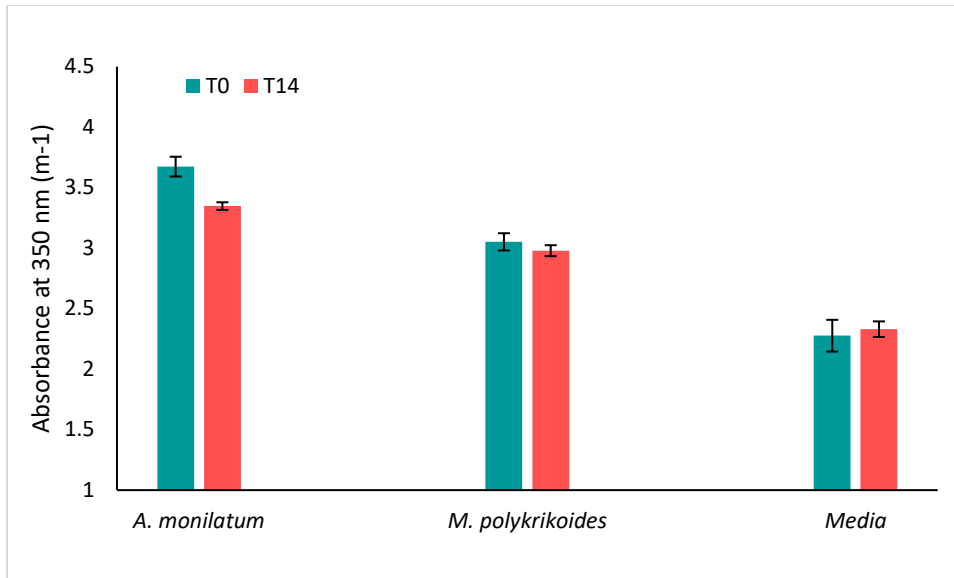
Figure 21: Comparison of the initial and final values for absorbance at 350 nm which was used as the measurement for CDOM for the microbial decomposition experiments. Error bars show one standard deviation.

ANOVA						
Source of Variation	*SS*	*df*	*MS*	*F*	*P-value*	*F crit*
Between Groups	5.879685	2	2.939842	253.6146	2.73E-12	3.68232
Within Groups	0.173877	15	0.011592			
Total	6.053561	17				

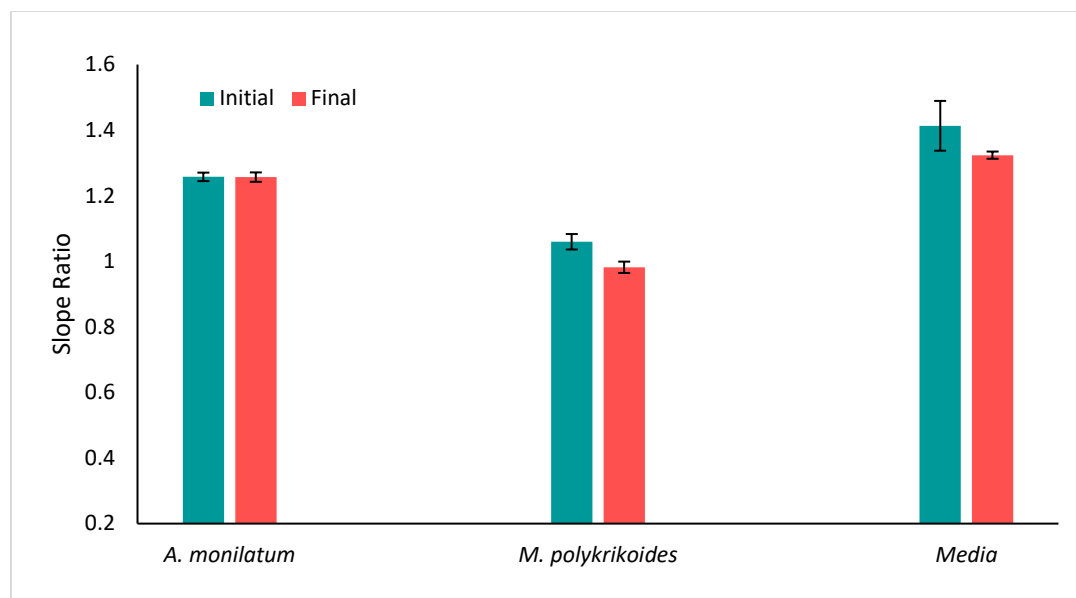Table 6: Single-factor ANOVA test comparing the initial Napierian absorption coefficients at 350 nm

Figure 22: Comparison of the initial and final values for S_R which was used as a proxy for molecular weight and photodegradability for the microbial decomposition experiments. Error bars show one standard deviation.

ANOVA						
Source of Variation	*SS*	*df*	*MS*	*F*	*P-value*	*F crit*
Between Groups	0.377026	2	0.188513	72.65139	1.92E-08	3.68232
Within Groups	0.038921	15	0.002595			
Total	0.415947	17				

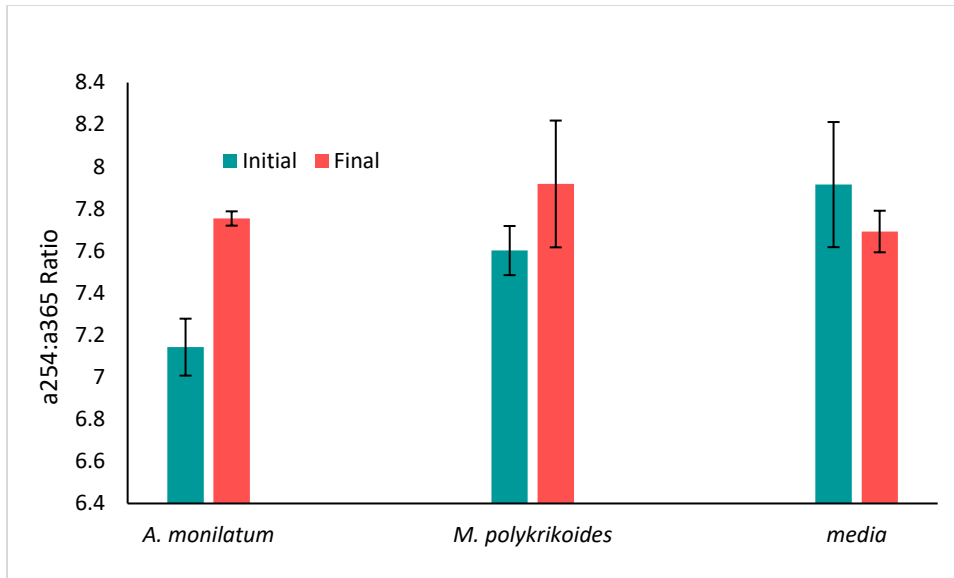Table 7: Single-factor ANOVA test comparing the initial SR values for the microbial decomposition experiments

Figure 23: Comparison of the initial and final values for $a254{:}a365$ which was used as a proxy for molecular weight for the microbial decomposition experiments. Error bars show one standard deviation.

ANOVA						
Source of Variation	*SS*	*df*	*MS*	*F*	*P-value*	*F crit*
Between Groups	1.810884	2	0.905442	18.80598	8.18E-05	3.68232
Within Groups	0.722197	15	0.048146			
Total	2.533082	17				

Table 8: Single-factor ANOVA test comparing the initial *a254:a365* values for the microbial decomposition experiments
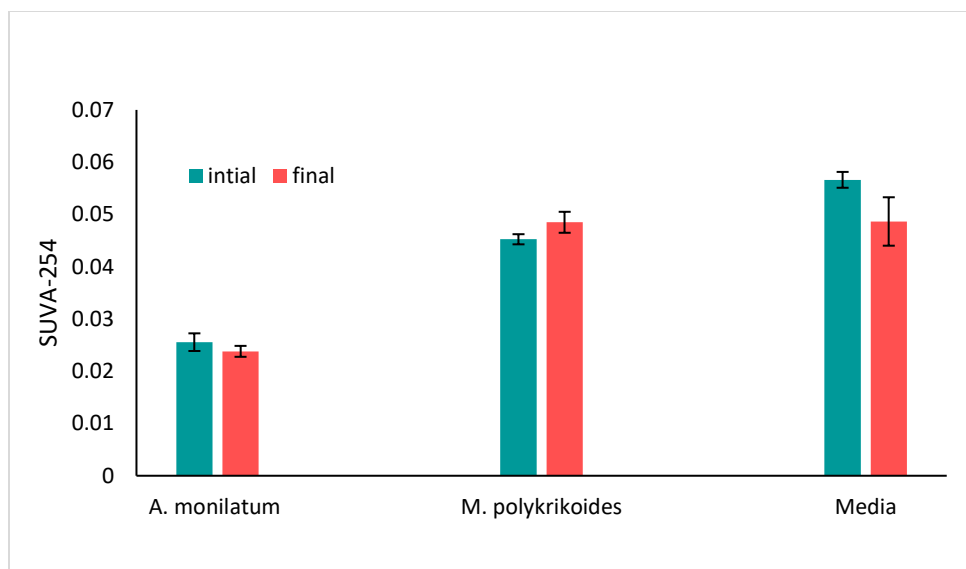
Figure 24: Comparison of the initial and final values for $SUVA_{254}$ which was used as a proxy for aromaticity for the microbial decomposition experiments. Error bars show one standard deviation.

ANOVA						
Source of Variation	*SS*	*df*	*MS*	*F*	*P-value*	*F crit*
Between Groups	0.001482	2	0.000741	242.98	1.81E-06	5.143253
Within Groups	1.83E-05	6	3.05E-06			
Total	0.0015	8				

Table 9: Single-factor ANOVA test comparing the initial values of $SUVA_{254}$ for the microbial decomposition experiments
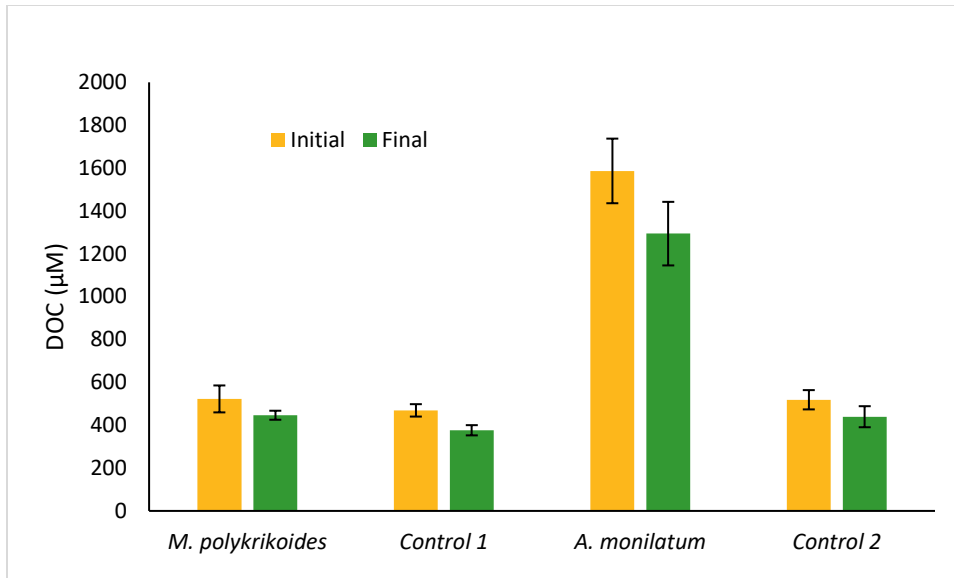
Figure 25: Comparison of initial and final DOC concentrations for the sediment core incubations. Control 1 was the control for the *M. polykrikoides* trial and control 2 was the control for the *A. monilatum* trial. Error bars represent one standard deviation.
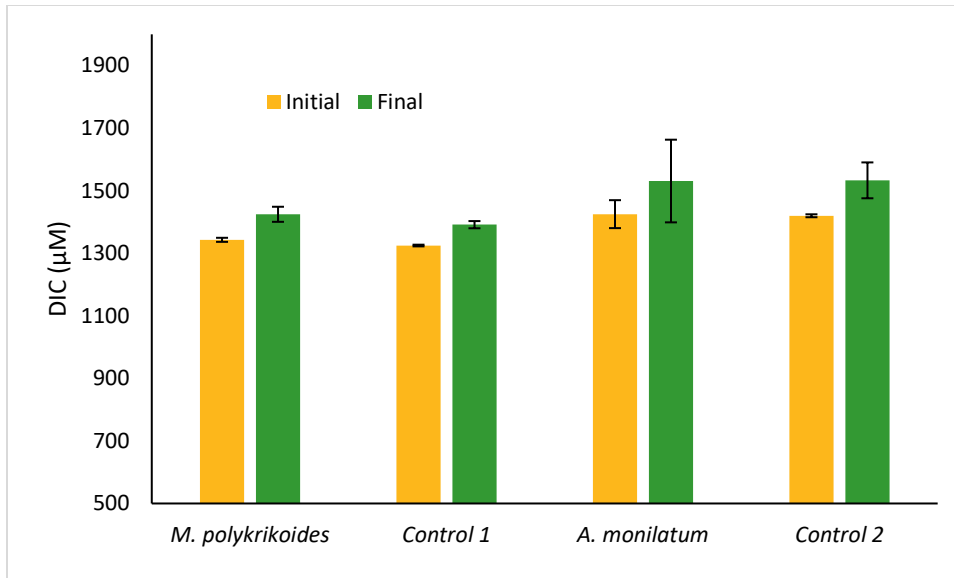
Figure 26: Comparison of initial and final DIC concentrations for the sediment core incubations. Control 1 was the control for the *M. polykrikoides* trial and control 2 was the control for the *A. monilatum* trial. Error bars represent one standard deviation.
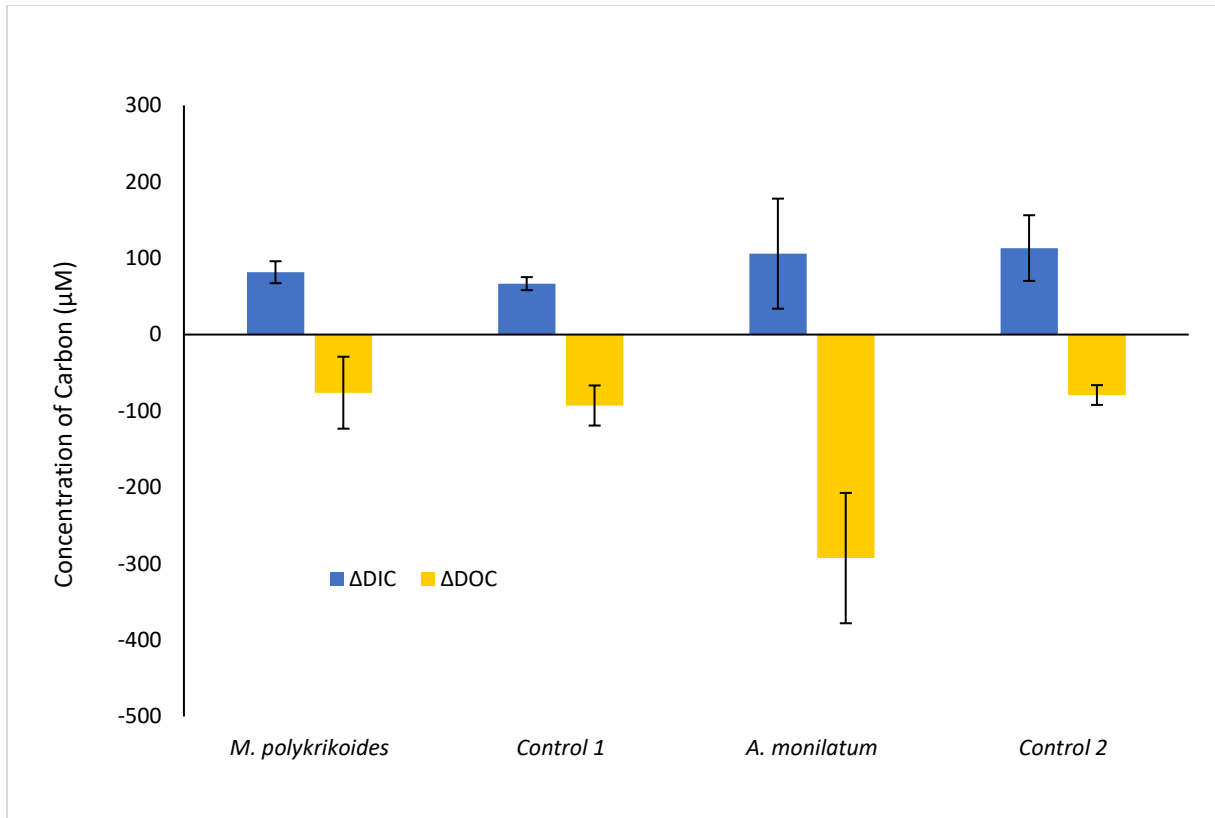
Figure 27: Comparison of the increase in DIC concentration (blue) to the decrease in DOC concentration (yellow) from initial to final samplings for the sediment core incubations. Control 1 was the control for the *M. polykrikoides* trial and control 2 was the control for the *A. monilatum* trial. Error bars represent one standard deviation.

ANOVA						
Source of Variation	*SS*	*df*	*MS*	*F*	*P-value*	*F crit*
Between Groups	4182.591	3	1394.197	0.50788	0.687744	4.066181
Within Groups	21961.05	8	2745.131			
Total	26143.64	11				

Table 10: Single-factor ANOVA test comparing the change in DIC concentrations after 6 hours for the sediment core incubations

ANOVA						
Source of Variation	*SS*	*df*	*MS*	*F*	*P-value*	*F crit*
Between Groups	99656.06	3	33218.69	8.555769	0.007059	4.066181
Within Groups	31060.85	8	3882.607			
Total	130716.9	11				

Table 11: Single-factor ANOVA test comparing the change in DOC concentrations for the sediment core incubation experiments.